

SLAC-PUB-5195

March 1990

(A)

**PROSPECTS FOR HIGH ENERGY  $e^+e^-$  LINEAR COLLIDERS\***

*R. B. Palmer*

Stanford Linear Accelerator Center, Stanford University, Stanford, CA 94309  
and Brookhaven National Laboratory, Upton, NY 11973

Submitted to *Annual Review of Nuclear and Particle Science*.

---

\* Work supported by Department of Energy contracts DE-AC03-76SF00515 (SLAC) and DE-AC02-76C0016 (BNL).

## TABLE OF CONTENTS

|     |   |    |
|-----|---|----|
| 1.  | INTRODUCTION . . . . .                                | 1  |
| 1.1 | <i>Proton-Antiproton Colliders</i> . . . . .          | 1  |
| 1.2 | <i>Circular Electron-Positron Colliders</i> . . . . . | 1  |
| 1.3 | <i>Linear Electron-Positron Collider</i> . . . . .    | 3  |
| 1.4 | <i>Plans for the Next Linear Collider</i> . . . . .   | 4  |
| 1.5 | <i>Acceleration Gradient</i> . . . . .                | 5  |
| 1.6 | <i>Required Luminosity</i> . . . . .                  | 7  |
| 1.7 | <i>The Luminosity Problem</i> . . . . .               | 8  |
| 2.  | INTERSECTION . . . . .                                | 10 |
| 2.1 | <i>Luminosity</i> . . . . .                           | 10 |
| 2.2 | <i>Crab Crossing</i> . . . . .                        | 11 |
| 2.3 | <i>Luminosity Pinch Enhancement</i> . . . . .         | 12 |
| 2.4 | <i>Disruption Angles</i> . . . . .                    | 13 |
| 2.5 | <i>Long-Range Kink Instability</i> . . . . .          | 15 |
| 2.6 | <i>Beamstrahlung</i> . . . . .                        | 16 |
| 2.7 | <i>Pair Production</i> . . . . .                      | 18 |
| 3.  | FINAL FOCUS . . . . .                                 | 21 |
| 3.1 | <i>Conventional Focusing</i> . . . . .                | 21 |
| 3.2 | <i>Synchrotron Radiation (Oide Limit)</i> . . . . .   | 22 |
| 3.3 | <i>Focusing Magnets</i> . . . . .                     | 23 |
| 3.4 | <i>Exotic Focusing</i> . . . . .                      | 24 |
| 4.  | LINAC . . . . .                                       | 26 |
| 4.1 | <i>Acceleration Structure</i> . . . . .               | 26 |
| 4.2 | <i>Traveling Wave Structures</i> . . . . .            | 27 |
| 4.3 | <i>Transverse Wakefields</i> . . . . .                | 30 |
| 4.4 | <i>BNS Damping</i> . . . . .                          | 31 |
| 4.5 | <i>Alignment Tolerances</i> . . . . .                 | 32 |

|     |   |    |
|-----|---|----|
| 4.6 | <i>Vibration Tolerances</i> . . . . .                   | 34 |
| 4.7 | <i>Longitudinal Wakes</i> . . . . .                     | 35 |
| 4.8 | <i>Multibunch Effects</i> . . . . .                     | 36 |
| 4.9 | <i>Field Limits</i> . . . . .                           | 38 |
| 5.  | RF POWER SUPPLY . . . . .                               | 39 |
| 5.1 | <i>Introduction</i> . . . . .                           | 39 |
| 5.2 | <i>Very High Voltage "Relativistic" Beams</i> . . . . . | 40 |
| 5.3 | <i>Wide or Multibeam Devices</i> . . . . .              | 42 |
| 5.4 | <i>Rf Pulse Compression</i> . . . . .                   | 43 |
| 5.5 | <i>Electrical Supply and Efficiency</i> . . . . .       | 44 |
| 6.  | ELECTRON AND POSITRON SOURCES . . . . .                 | 46 |
| 6.1 | <i>Electron Source</i> . . . . .                        | 46 |
| 6.2 | <i>Positron Source</i> . . . . .                        | 46 |
| 6.3 | <i>Damping Ring</i> . . . . .                           | 47 |
| 7.  | EXAMPLES . . . . .                                      | 51 |
| 7.1 | <i>Introduction</i> . . . . .                           | 51 |
| 7.2 | <i>Assumptions</i> . . . . .                            | 51 |
| 7.3 | <i>Philosophies</i> . . . . .                           | 54 |
|     | 7.3.1 SINGLE BUNCH DESIGNS . . . . .                    | 54 |
|     | 7.3.2 MULTIPLE BUNCH DESIGNS . . . . .                  | 56 |
| 7.4 | <i>Designs as a Function of Energy</i> . . . . .        | 59 |
| 7.5 | <i>Energies Above 10 TeV?</i> . . . . .                 | 61 |
| 8.  | CONCLUSION . . . . .                                    | 62 |
|     | <i>Literature Cited</i> . . . . .                       | 64 |
|     | <i>Table 1</i> . . . . .                                | 71 |
|     | <i>Table 2</i> . . . . .                                | 73 |
|     | <i>Table 3</i> . . . . .                                | 75 |
|     | <i>Figure Captions</i> . . . . .                        | 77 |

## 1. INTRODUCTION

### 1.1 *Proton-Antiproton Colliders*

High energy physicists study the microstructure of the universe by observing the products of collisions of fundamental particles. To study ever-smaller distances they require ever-higher collision energies. The proton-antiproton collider at the Fermi National Accelerator Laboratory (FNAL), is currently the highest energy such machine. It can attain a center of mass energy of nearly 2 TeV ( $2 \times 10^{12}$  electron volts). The Superconducting Supercollider (SSC), now under construction, will be a proton-proton machine and will reach an energy of 40 TeV.

These machines are circular and use magnets to bend the particles (protons or antiprotons) round the two arcs in opposite directions [Figure 1(a)]. Acceleration is provided by rf (radio frequency) cavities, but since the acceleration can be given during many revolutions, these cavities are not a crucial element. Since there is a technical limit to how high the bending magnetic fields can be, the diameters rise more or less linearly with the energy. Figure 2, line (b) shows the circumference against energy for some representative machines. The higher-energy machines use somewhat higher magnetic fields and are thus not quite so large, but the enormous forces and higher costs involved in high fields preclude any radical reduction in size. The SSC will have a circumference of over 70 km. To attain higher energies by making even larger machines seems impractical. One seeks other approaches.

### 1.2 *Circular Electron-Positron Colliders*

One alternative approach to higher energies is to construct circular electron-positron colliders [Figure 1(b)]. With such colliders a larger fraction of the collision energy is available for study, so a machine of this type with the same total collision energy as a proton machine could probe higher energy phenomena. The reason for this is that protons (the nuclei of hydrogen) and antiprotons are complex structures, made

up several of the more fundamental quarks and gluons. When two of these protons or antiprotons collide, most of the quarks and gluons in the two colliding particles will not be strongly involved in the collision, and will fly on past one another. The "available energy" for making new phenomena will only be that arising from the collision of one constituent from each particle, and that energy will be only a fraction of the total that was, "in principle," available. How small that fraction is can only be stated qualitatively; there is always a very small probability of a very large fraction, but it is of the order of one-tenth (this factor was used in the left hand scale of Figure 2).

In contrast to the protons and antiprotons, electrons and positrons are, as far as we know, fundamental point-like objects. If an electron and positron collide, all the energy in the two particles is available for generating new phenomena. Thus an electron-positron collider with the same beam energy as a proton-antiproton collider would have an "available energy" ten times as great.

Why then do we build proton-antiproton colliders? Why not always construct electron-positron machines of the same energy? The problem is synchrotron energy loss. In the proton-antiproton machines the particles are bent round the huge rings by high field superconducting magnets. This works fine for the relatively heavy protons and antiprotons, but if the same were tried with the light electrons their velocity would become so high that they would radiate energy faster than the rf accelerating cavities could replenish it.

A simple scaling relation for circular electron colliders is instructive. The synchrotron radiation energy loss per revolution round a ring of radius  $R$  is proportional to  $E^4/R$ , where  $E$  is the energy of the electrons. Since the rf acceleration to make up the synchrotron energy loss will become a major cost, we can approximate the total

cost of the facility by:  $\$ = \text{const} \times R + \text{const} \times E_{\text{loss}}$ . It is easy to see that the cost is a minimum when the cost of radius and energy loss are equal, and the radius and cost are then proportional to the square of the energy.

In Figure 2 (line a) the circumferences and energies of a number of representative electron-positron colliders are given. As predicted, the size rises approximately as the square of the energy. At low energies the size needed for a given "available energy" is less than for proton machine (line b), but at higher energies an electron machine is much larger and more expensive.

### 1.3 Linear Electron-Positron Collider

The solution to the synchrotron radiation problem is to build electron-positron linear colliders [Figure 1(d)]. Since the accelerators are linear, there are no bending magnets and no synchrotron radiation. However, since the particles pass through the rf cavities only once, the full machine energy must be provided by the cavities. High accelerating fields are required, and the machines will tend to be very long. Such a machine was first proposed, but for low energies, by Tigner (1). Amaldi (2) was the first to discuss a linear collider for high energies. He proposed to use superconducting cavities and an energy recovery scheme. A proposal made by Novosibirsk (3) used a conventional linac and several other now standard features, including flat beams. Then, at the International Committee for Future Accelerators (ICFA) workshop in 1978, held at Fermilab (4), many ideas were studied, including that of using the existing Stanford Linear Accelerator Center (SLAC) to drive a pseudo-linear collider. This concept is now known as the Stanford Linear Collider (SLC) (5) (see Sec. 7.4, Table 3, column M).

The SLC is now operating (6). A single linear accelerator is used to accelerate both the electrons and the positrons. The two beams are then divided and bent

around two arcs to collide head-on in the interaction region [Figure 1(c)]. At higher energies the synchrotron radiation in these arcs would be intolerable, but this machine, with a center-of-mass energy of 100 GeV, is just below such an energy. Indeed at this energy it is still quite practical to build a circular machine, such as the Large Electron-Positron (LEP) collider at the Center European for Research Nuclear (CERN), Switzerland. Because of these arcs, the SLC is not a true linear collider. It is an adaptation of a previously existing machine. As a result, its luminosity is somewhat limited, but it has proven all the fundamental assumptions, and has taught us many painful lessons on what is needed for the designs of the future.

#### *1.4 Plans for the Next Linear Collider*

There are now four possible plans for a next linear collider:

1. In Protvino, near Moscow, plans are well advanced for the construction of VLEP (7). This machine is the current embodiment of the proposal first made by the Novosibirsk group (3). Its first phase would have an energy of 0.3 TeV, accelerating gradient of 100 MeV/m, and thus a length of the order of 3 km.
2. At SLAC energetic research and development is going on, and the director has stated his intent to submit a proposal for a true linear collider within a few years. The early work was aimed at a center-of-mass energy of 1 TeV (1000 GeV), to be called the TeV Linear Collider (TLC). It would have about 200 MeV/m acceleration, and a length of about 6 km. A phase one, intermediate Linear Collider (ILC), would have half that energy, a gradient of about 100 MeV/m, and the same length.
3. The Japanese high energy physics lab (KEK) is collaborating closely with SLAC, and doing extensive additional work. Their ideas are similar to those at

SLAC, aiming for a phase one machine with 100 MeV/m gradients and 400 GeV total energy. Their director has stated that a proposal should be expected soon.

4. A research and development program has also been underway at CERN, with the specific aim of a 2 TeV center-of-mass energy, to be known as the "CERN Linear Collider" (CLIC) (8). However, the director there is favoring a different project, and has stated no firm intent to submit a proposal.

The existing SLC is about 3 km long and has a center-of-mass energy of 100 GeV. This [plotted on Figure 2(c)] is longer than a comparable proton or antiproton machine. But the next-generation linear collider, as discussed above, is likely to employ a gradient of around 100 MeV/m, have an energy of about 500 GeV and thus an overall length of the order of 6 km. This (also plotted on Figure 2) would have less length per available energy than any other collider type. The phase two SLAC TLC design would continue this trend. How far can it continue?

### 1.5 Acceleration Gradient

The maximum acceleration gradient  $G_{max}$  is limited, in conventional structures, by breakdown and dark current (see Sec. 4.9). It is not known exactly what the ultimate limit is, but it seems to be given approximately by:

$$G_{max} \propto \lambda^{-1/2} t^{-1/4} \quad . \quad 1.$$

If a pulse length  $t$  equal to the loss time  $\tau$  is assumed, where  $\tau \propto \lambda^{1.5}$  then the breakdown limit would be given by

$$G_{max} \propto \lambda^{-7/8} \quad . \quad 2.$$

This limit is shown on Figure 3(a). It is seen that, at a wavelength of 2.5 cm, the gradients of 80–200 MeV/m, as proposed in the above machines, are not unreasonable.

For a future 5 TeV machine, with a wavelength of perhaps 1 cm, a value of 300 MeV/m is not unthinkable.

As the figure shows, higher gradients are possible at optical wavelengths (9), or with single electromagnetic pulses generated by "switched power" (10), or wake-fields (11). Clearly, in plasmas, the above breakdown limits do not apply and even higher gradients are possible (12,13). Nor do they apply in a vacuum, far from any material. Acceleration, in this case, is still possible in the presence of magnetic fields (14). Several of these ideas could certainly achieve gradients of several GeV per meter, thus shrinking the collider lengths dramatically. Unfortunately, considerations of luminosity (see Sec. 1.7) argue against the use of most, if not all, of the above "exotic" acceleration schemes.

It is also not obvious that the highest gradient will yield the most economical collider. In any electromagnetic accelerator the electromagnetic energy needed per pulse per unit length will be proportional to the square of the accelerating field, and thus the total energy needed will be linear with the field. Since the generation of this energy is, in general, expensive, the most economical machine will involve a trade-off between linear and power source costs, and will dictate the most economical gradient. Figure 4 shows lines of constant costs on an accelerating gradient vs. wavelength plot. The dashed line represents that gradient that would give a minimum cost at that wavelength. One notes that this gradient rises, and the total cost falls, as the wavelength gets shorter. Again we would conclude that very short wavelengths are favored, but this is complicated by the higher cost and lower efficiency of power sources at very short wavelengths. In addition one finds that considerations of luminosity and tolerances argue against short wavelengths.

## 1.6 Required Luminosity

High-energy colliders are built to study high-energy phenomena, that is, the production and decay of high-energy states. Unfortunately, as a consequence of quantum mechanics, there is an inevitable relationship between the energy of a phenomenon and its characteristic size and cross section  $\sigma$ .

$$\sigma \propto E^{-2} \quad , \quad 3.$$

where  $E$  is the energy of the phenomenon (i.e., the center-of-mass energy of the fundamental collision). The cross section  $\sigma$  of a phenomena tells us what luminosity  $\mathcal{L}$  (related to the flux of colliding particles) is needed to achieve a given average rate  $dn/dt$  of its occurrence:

$$\frac{dn}{dt} = \mathcal{L} \sigma \quad . \quad 4.$$

If we require a given rate of phenomena, independent of energy, then clearly we need a luminosity that rises as the square of the energy. The situation is illustrated by Figure 5. The plot shows the luminosity of some representative electron-positron colliders versus their center-of-mass energies. The line represents a rate of 10,000 events per year (defined as  $10^7$  seconds) per unit of  $R$ , where  $R$  is the ratio (of the order of unity) of cross sections to that of the reaction  $e^+ e^- \rightarrow \mu^+ \mu^-$ . We see that in going from the SLC to a 1 TeV collider (TLC), the energy increase needed is only 10, compared with the needed luminosity increase of 5000. For a 10 TeV collider the luminosity increase required is 500,000.

Some might settle for a factor of 10 less than 10,000 events per year per unit of  $R$ . But since the actual performance of any linear collider is likely to fall below its design (as is the case now with the SLC) it would be unwise to design future machines for lower luminosities.

## 1.7 The Luminosity Problem

The luminosity of a collider is given by:

$$L \propto \frac{f N^2}{A} , \quad 5.$$

where  $f$  is the frequency of bunches colliding,  $N$  is the number of colliding particles per bunch, and  $A$  is the average transverse cross section of the intersecting beams. As we shall see, there is a limit to how small  $A$  can be made, that depends on the emittance  $\epsilon_n$  of the beams. And there is a limit on how large an  $N$  can be used without introducing unacceptable energy spread in the collision. Given these limits, higher luminosity can only be achieved by using a higher frequency  $f$ . But a higher frequency implies a higher average current. If the luminosity is to rise as the square of energy, then the average power will be seen to rise as the cube of that energy. At some point this becomes a limiting expense. Indeed we find that this, rather than the simple collider length, is the real problem at energies above about 1 TeV. The criteria we then look for, rather than pure acceleration gradient, become:

1. Design of the final focus and intersection region to maximize luminosity for given beam power.
2. The design of an electromagnetic power supply with low cost and high efficiency of converting wall power to rf electromagnetic power.
3. Use of an acceleration scheme with high efficiency for conversion of rf electromagnetic power to beam power.
4. Use of an acceleration scheme with the ability to transport very low emittance beams without dilution.
5. Design of a source of electrons and positrons with the lowest possible emittance.

6. And, only when the above considerations are satisfied, use of the highest possible accelerating gradient consistent with minimizing the cost.

Damping rings can and, if the higher luminosities are to be reached, must produce normalized emittances of the order of  $10^{-8}$  mrad, in at least the vertical direction. Because of the need to transport such small emittances, we find that the above criteria do not favor any acceleration mechanism with strong transverse fields, thus excluding all systems using plasmas (12, 13) or other mediums [strong transverse fields exist in conventional cylindrically symmetric structures, but, as a result of the Panofsky-Wenzel Theorem (15), these fields add to give zero transverse deflections].

Transverse wakefields, left by the front of the accelerated bunch, which act on the tail, can also be a problem, but are correctable by an introduced momentum spread between the head and tail of each bunch (see Sec. 4.4). But this momentum spread will itself cause emittance blow up unless stringent alignment requirements are met. The shorter the wavelength, the worse the wakefields, the greater the momentum spread needed and the worse the alignment problem. As a result, one finds that very short, such as optical, wavelengths (9) are strongly disfavored. And in addition, optical power sources, such as lasers, are not favored because of their low efficiency.

Inverse Free Electron Lasers (15), even at short wavelengths, do not have any transverse wakefields, but they cannot be used because the synchrotron radiation in their magnetic fields results in severe energy loss and emittance blow up.

Single pulse devices, such as nonplasma wakefield (11) or switched power (10) accelerators, do not intrinsically suffer from special emittance preservation problems, but the requirement of cylindrical field symmetry may be hard to achieve. And, since they do not benefit from the resonant energy accumulation over a significant fill time, they are likely to suffer higher power source costs.

I am thus forced to conclude that, with the possible exception of single pulse devices, none of the “exotic” acceleration mechanisms is, or will ever be, suitable for high-energy linear colliders. One must be careful making such statements. New inventions, or even new optimizations, might lead to different conclusions. But it is hard, at this time, to see how.

The requirements for luminosity do favor superconducting accelerators (16). The wavelengths of such structures can be large, making the wakefields negligible. The damping time being essentially infinite, rf power can be fed continuously from a low-power, high-efficiency source. Unfortunately, at this time, the highest accelerating gradient that can be realistically achieved is only about 7 MeV/m, and that is just too low. However, the true limit (achieved in small single cavities) is about 40 MeV/m for niobium, and may be as high as 400 MeV/m for the new high temperature superconductors. If such fields could be achieved, then superconducting structures would be highly desirable.

But, for the moment, only room-temperature conventional linac structures appear to be practical, and so, in what follows, I will restrict myself to a collider design based on such structures.

## 2. INTERSECTION

### 2.1 Luminosity

When the two bunches collide, the luminosity obtained is

$$\mathcal{L} = \frac{N^2 f H_D}{4\pi \sigma_x \sigma_y} \eta_L \quad , \quad 6.$$

where  $N$  is the number of particles per bunch,  $f$  is the bunch repetition frequency,  $H_D$  is a pinch enhancement factor that will be discussed in Sec. 2.3, and

$$\sigma_{x,y} = \left( \frac{\epsilon_{x,y} \beta_{x,y}^*}{\gamma} \right)^{1/2} . \quad 7.$$

$\eta_L$  is an efficiency factor to allow for effects of both a finite angle of crossing and a  $\beta^*$ , if it is not very much larger than the bunch length  $\sigma_z$ .

$$\eta_L = \frac{2}{\sigma_z \sqrt{\pi}} \int_0^{\infty} \frac{\exp \left\{ - \left( \frac{z}{\sigma_z} \right)^2 \left[ 1 + \frac{\theta_{int}^2}{\theta_d^2} \left( \frac{1}{1 + (z/\beta_x)^2} \right)^2 \right] \right\}}{\left( 1 + (z/\beta_y)^2 \right) \left( 1 + (z/\beta_x)^2 \right)} dz , \quad 8.$$

where  $\theta_d = \sigma_x/\sigma_z$  is the diagonal angle,  $\beta_x$  and  $\beta_y$  are the  $\beta^*$ 's at the final focus in the two directions. In a conventional finite angle crossing  $\theta_{int}$  is the crossing angle  $\theta_c$ . In this case, if  $\theta_c$  is much greater than the diagonal angle  $\theta_d$  then there is a severe loss of luminosity. This can, however, be avoided by "crab crossing" in which case  $\theta_{int} = 0$ , independent of  $\theta_c$ .

## 2.2 Crab Crossing

In crab crossing (17) (see Figure 6), rf-driven deflecting structures are introduced just before or after the final focusing magnets of each beam. The phasing of the rf is such that the center of each bunch is undeflected, the front shifted to one side, and the back to the other such as to introduce a tilt of  $\theta_c/2$  in the bunch with respect to its direction of motion (the bunches move in a partially "crab"-like way). The sign of the tilts are such that the two bunches are "in line" as they cross. In their own center of mass, they interact with zero crossing angle and suffer no luminosity loss. The integrated deflection fields of the deflecting structures  $V_{trans}$  is given by:

$$V_{trans} = \frac{\theta_c \lambda E}{4 \pi F_x} , \quad 9.$$

where  $\lambda$  is the rf wavelength,  $E$  is the beam energy in electron volts, and  $F_x$  is the horizontal focal length of the final focusing system. For realistic cases this voltage can easily be achieved in a structure of a meter or so length. The only serious problem is that the phase of the two deflectors must be very well controlled. If they are driven from the same source, this should not be a problem.

### 2.3 Luminosity Pinch Enhancement

$H_D$  in Eq. 6 is an enhancement factor due to the pinch effect. It is a function of  $A = \sigma_z/\beta^*$ , of any offset  $\delta y$ , and of a disruption parameter  $D_y$ , defined by

$$D_y = \frac{\sigma_z}{F} \quad , \quad 10.$$

where  $F$  is the effective focal length of the pinch focusing of one bunch by the other, calculated for the center of short Gaussian bunches.

Assuming a beam in which  $\sigma_x \geq \sigma_y$ , then Wilson (18) has shown that

$$D_y \approx \frac{r_e N \sigma_z}{\gamma \sigma_y^2} \cdot \frac{2}{1 + \frac{\sigma_x}{\sigma_y}} \quad . \quad 11.$$

The enhancement  $H_D$  has been calculated by Chen & Yokoya (19) and is discussed in the review by Chen (20). For  $\delta y = 0$ , the enhancement for round beams is shown in Figure 7, and for flat beams in Figure 8.

For round beams, the enhancement is given approximately by

$$H_D(\text{round}) = 1 + D_y^{1/4} \left( \frac{D^3}{1 + D^3} \right) \left( \ln(D_y^{0.5} + 1) + 2 \ln \left( \frac{0.8}{A} \right) \right) \quad , \quad 12.$$

and for flat beams

$$H_y(\text{flat}) \approx [H_D(\text{round})]^{1/3} \quad . \quad 13.$$

These plots and approximate formulae show that, for  $\delta y = 0$ , as  $D_y$  increases, so the enhancement will increase without limit. This is true if the two beams are in perfect alignment with one another. In practice, a kink instability sets in, that strongly reduces the enhancement, even for infinitesimal misalignments  $\delta y$ , at large values of  $D_y$ . As a result of this effect, there is a de facto limit on  $H_D$  reached when the disruption parameter  $D_y$  has a value of about 20.

The kink instability is not, however, all bad. At low values of the disruption parameter  $D_y$ , it results in a decrease in sensitivity to any offset by an amount  $C_D$ , which is relatively insensitive to  $A$ .  $C_D$  is defined by the displacement needed to generate the same luminosity loss as that given by a one standard deviation displacement, and is given approximately by:

$$C_D \approx \left( \frac{1}{1 + 0.2D} \right)^2 + \left( \frac{D^2}{240} \right)^2 \quad 14.$$

The decrease is maximal for  $D_y$ 's in the region of 5 to 10 (see Figure 9), and corresponds to a lessening of the expected sensitivity to offsets by a factor of 2. Above a  $D_y$  of 20, the sensitivity rises dramatically, as the instability asserts itself.

#### 2.4 Disruption Angles

The disruption process, not only improves the luminosity, but also increases the divergence  $\theta_D$  of the beam. At low energies, before the onset of quantum effects, this divergence will be important. In a head-on geometry ( $\theta_c = 0$ )  $\theta_D$  will set the aperture of the opposite beam focusing quadrupoles. In a finite angle crossing geometry, it will set the required crossing angle.

The maximum *disruption angle* is given (21) by

$$\hat{\theta}_D(x, y) = \frac{2Nr_e}{\gamma\sigma_x} \cdot k_{x,y} H_\theta \quad , \quad 15.$$

where for  $\sigma_x = \sigma_y$

$$k \approx 0.45 \quad , \quad 16.$$

and for  $\sigma_x \gg \sigma_y$

$$k_x \approx 0.75 \quad \text{and} \quad k_y \approx 1.25 \quad . \quad 17.$$

The situation is somewhat different in the three cases. For  $\theta_x$  and for  $\theta_y$  in round beams, a well-defined maximum angle occurs for particles at a finite impact parameter near  $\sigma$ . But for  $\theta_y$  in flat beams, the deflecting field rises to a plateau and the maximum angle occurs only for particles in the extreme tail of the distribution. As a result, the mean value is much less in this case.

With pinch, the situation has again been studied by Chen & Yokoya. At small values of the disruption parameter  $D_y$  the disruption angles are enhanced, but for larger  $D_y$  (of the order of 1 and above for round beams, and of the order of 5 and above for flat beams) the disruption angles are suppressed. Initially the particles oscillate in the pinch fields of the oncoming beam, but the amplitude of this oscillation is adiabatically damped as the particle leaves the pinch field of the oncoming bunch.

For values of  $D_y$  above one, the enhancement of the maximum disruption angles is found to be little dependent on  $A$  and is given approximately by (for round beams):

$$H_\theta \approx 1 / \left( \left[ \frac{1}{1.2 + 50D^3} \right] + \left[ 0.06 + \frac{D}{3.38} \right]^{0.5} \right) \quad , \quad 18.$$

and for flat beams:

$$H_{\theta_{x,y}} \approx \frac{1.0}{[1 + (0.5D_{x,y})^5]^{1/6}} \quad . \quad 19.$$

In this discussion, I have not included quantum fluctuations in the disruption process. At high energies, there is a finite probability that an electron radiates a hard photon and is then, because it has a low momentum, disrupted by a much larger angle:

$$\theta_D(\text{quantum}) = \theta_D \left( \frac{E_e}{E_e - E_\gamma} \right) \quad . \quad 20.$$

The factor  $E_e/(E_e - E_\gamma)$  can be large and the resulting disruption would be a problem at collider energies above 1 TeV, if it were not for the presence of a yet more serious one: pair production, which will be considered later.

### 2.5 Long-Range Kink Instability

There is a long-range kink instability that arises when more than one bunch is colliding with more than one bunch from the other direction. This, of course, is only possible at all when the bunches are crossing at a finite angle. This kink instability sets a lower limit on this crossing angle.

The instability was first noted by Yokoya & Ruth (22), and is discussed in Chen's review (20). As the  $n$ 'th bunch approaches the intersection point, it must pass  $n^{-1}$  bunches, from the other beam, that have already interacted. If the first bunches are misaligned, they leave the intersection point deflected. Later bunches, as they pass these outgoing deflected bunches, are themselves further displaced, and, after they have intersected, leave at even greater deflection angles. The situation is unstable and the growth rate must be kept very low.

The approximate condition for growth  $C_n$  of the instability by not more than a factor of 2 is:

$$\left( \frac{1}{1 + D_y/4} \right) D_y^2 \left( \frac{\sigma_y}{\sigma_x} \right) \left( \frac{\theta_d}{\theta_c} \right)^2 \leq 2 \quad . \quad 21.$$

In a normal crossing situation, there will be a severe loss of luminosity if  $(\theta_d/\theta_c) < 1$  and the above requirement reduces to

$$\left( \frac{1}{1 + D_y/4} \right) D_y^2 \left( \frac{\sigma_y}{\sigma_x} \right) \leq 2 \quad . \quad 22.$$

which is a serious restriction. However, with crab crossing (see Sec. 2.2) Eq. 21 can easily be satisfied, and the restriction of Eq. 22 no longer applies.

### 2.6 *Beamstrahlung*

Beamstrahlung is the synchrotron radiation produced by the particles of one bunch as they pass through the magnetic and electric fields of the oncoming bunch. The fields are so high that the classical formulae are not sufficient and we must use the quantum results first given by Sokolov & Ternov (23), and first applied to the bunch crossing situation by Himel & Siegrist (24). Much work has been done confirming the approximations used (25).

Here, I take the calculations from Noble (26). The fractional loss of energy  $\delta$  of one bunch passing through the other is given by

$$\delta \approx \frac{F_1 r_e^3 N^2 \gamma}{\sigma_z (\sigma_y')^2} \left[ \frac{4}{\left( 1 + \frac{\sigma_x'}{\sigma_y'} \right)^2} \right] H_T \quad , \quad 23.$$

where

$$\sigma_x' = \frac{\sigma_x}{H_x} \quad , \quad \text{and} \quad \sigma_y' = \frac{\sigma_y}{H_y} \quad , \quad 24.$$

$F_1 \approx 0.22$ ,  $r_e \approx 2.82 \times 10^{-15}$  m, and the enhancement factors  $H_{x,y}$  have been introduced to give an approximate allowance for the disruption pinch.

In the symmetric case,  $H_x H_y = H_D$ . For a flat beam,  $\sigma_x \gg \sigma_y$  and  $H_x \approx 1$  and:

$$\delta \approx \frac{F_1 r_e^3 N^2 \gamma}{\sigma_z} \frac{4}{(\sigma_x)^2} H_\Upsilon, \quad 25.$$

and is not a function of  $\sigma_y$  or  $D$

The parameter  $H_\Upsilon$  in Eqs. 23 and 25 is a correction for quantum effects:

$$H_\Upsilon \approx \left( \frac{1}{1 + 1.33 \Upsilon^{2/3}} \right)^2, \quad 26.$$

where

$$\Upsilon = \frac{F_2 r_e \lambda_e \gamma N}{2 \pi \sigma_z \sigma_y'} \left[ \frac{2}{1 + \frac{\sigma_x'}{\sigma_y'}} \right]; \quad 27.$$

$F_2 \approx 0.43$ ,  $r_e \approx 2.82 \times 10^{-15}$ , and  $\lambda_e \approx 3.86 \times 10^{-13}$  m. Note again that I have expressed  $\Upsilon$  as a function of the effective spot dimensions  $\sigma_x'$  and  $\sigma_y'$ . And we also note again that for  $\sigma_x' \gg \sigma_y'$ ,  $\Upsilon$  is a function only of  $\sigma_x'$  and that this is *not* significantly enhanced by pinch. This is a reflection of the fact that the fields in a flat beam are a function of the width of that beam, but not of its vertical thickness.

$H_\Upsilon$  is seen to suppress the beamstrahlung for high values of  $\Upsilon$  (see Figure 10), but examination of Eqs. 23, 25 and 27 will show that the  $\gamma$  and bunch length dependence of  $\delta$  is proportional to  $\Upsilon H_\Upsilon$  which has a maximum for the region near  $\Upsilon \approx 1$ , (see Figure 10). This region is approximately that for any practical 0.5–1 TeV collider (see Sec. 7.4), so choice of bunch length has little effect. But for a 10 TeV collider, short bunch lengths are favored.

## 2.7 Pair Production

There are three different pair production mechanisms that dominate at different energy regimes:

1. At low energies, where  $\Upsilon < 0.6$ , pairs are made by the incoherent interaction of beamstrahlung photons on individual particles in the oncoming beam. This process was first identified by Zolotarev, Kuraev & Serbo (27), and discussed by Telnov et al (28).
2. At energies where approximately  $0.6 < \Upsilon < 100$ , pair production is dominated by a coherent process, first noted by Chen (29). In this case the beamstrahlung photons are converted in the strong field of the entire oncoming bunch.
3. The third process, which dominates only at  $\Upsilon > 100$ , is the coherent direct trident production  $e^\pm \rightarrow e^\pm e^+ e^-$  induced by the field of the oncoming bunch. This is discussed by Chen & Telnov (30).

These processes have also been discussed in a number of publications since Ref. (31).

In all cases, the particles produced can become a serious background. The members of the pairs of the same sign as the beam that generated them are less of a problem. As in the case of the disrupted particles, they are focused by the fields of the oncoming beam, and tend to emerge at relatively small angles. The particles of the opposite sign, however, are defocused by these fields, and can emerge at larger angles. They may then hit the pole tips of the opposite focusing magnets. If there were only a few such pairs, this might not be a problem, but the production can become prodigious, and the backward "spray," or albido, from the collision of these particles with the poles could present a serious background problem.

The cross section for the incoherent process (Point 1 above) is given by:

$$\sigma(\gamma e \rightarrow ee^+e^-) \approx \frac{28}{9} \alpha r_e^2 \log \left( \frac{2 E_\gamma E_e}{m^2 c^4} \right) , \quad 28.$$

where  $\alpha$  is the fine structure constant,  $E_\gamma$  is the energy of the photon,  $E_e$  is the energy of the pair electron or positron,  $m$  is the electron mass, and  $c$  is the velocity of light. For a typical TeV collider, this cross section is of order  $6 \times 10^{-26}$  cm<sup>2</sup>, and the number of such pairs is of the order of  $2 \times 10^5$ , a not-negligible number.

The cross section for the coherent processes (Points 2 and 3 above) can be given in terms of the number of pairs  $n$  produced per initial electron or positron in the beams:

$$n_b(e \rightarrow e\gamma, \gamma \rightarrow ee) \approx 0.088 \left( \frac{\alpha \sigma_z}{\gamma \lambda_c} \Upsilon \right)^2 \Xi(\Upsilon) , \quad 29.$$

$$n_\nu(e \rightarrow eee) \approx 0.088 \left( \frac{\alpha \sigma_z}{\gamma \lambda_c} \Upsilon \right) \Omega(\Upsilon) , \quad 30.$$

where  $\alpha \approx (1/137)$ ,  $\lambda \approx 3.86 \times 10^{-13}$ , and  $\Upsilon$  is given by Eq. 27. Approximate expressions for  $\Xi$  and  $\Omega$  are given in Ref. 30 and are plotted in Figure 11.

For a typical fractional energy loss  $\delta$  of about one-sixth, for  $\Upsilon < 0.6$  the coherent (Point 2 above) contribution  $n_b$  is less than  $10^{-5}$ , and thus less than the incoherent contribution. Above that value of  $\Upsilon$ ,  $n_b$  rises rapidly to of the order of 1/100 and remains approximately at that level. This implies that for a typical bunch of  $10^{10}$  particles, of the order of  $10^8$  pairs are generated from the real beamstrahlung photons.

For a typical fractional energy loss  $\delta$  of one-sixth, the relative magnitudes of the real and virtual photons (Points 2 and 3 above) are as for the auxiliary functions of Figure 11, and we see that the virtual photon contribution is less than that of the real photons for all  $\Upsilon$ 's less than  $10^4$ .

The numbers of pairs produced can be so large that it is imperative that they not be allowed to hit any material. We must examine therefore the energy and angular distribution of these electrons, and discuss how they can be funneled out of the experimental region.

The energy distribution of the electrons is controlled by that of the beamstrahlung photons that generate them. This distribution falls (as in the classical case) as  $(E_\gamma)^{2/3}$ , but is cut off (from the quantum considerations) at  $E_{beam}$ . Thus the number of pair electrons below an energy  $E$  is approximately

$$n(\leq E) \approx n \left( \frac{E}{E_{beam}} \right)^{1/3} .$$

For example, for a beam energy of 500 GeV, the fraction of pairs below 250 MeV would be 8%, and the numbers of electrons produced would still be large, of the order of 16,000 for a typical TLC case ( $\Upsilon < 0.6$ ), and of the order of  $10^7$  in a multi-TeV collider.

The very high energy pairs are not a problem because they are emitted only in the forward direction, and will exit with the beam. The lower-energy electrons from the pair are, however, deflected by the fields generated by the other bunch. One sign is focused in but the other sign is deflected out. The angle of the outward deflected electron is given approximately by

$$\Theta_p \approx 1.5 \left( \frac{r_e N}{\gamma \sigma_z} \right)^{1/2} , \tag{31}$$

where  $N$  is the number of electrons in the oncoming bunch,  $\gamma$  is the gamma of the outgoing electron or positron, and  $\sigma_z$  is the rms bunch length. For a 250 MeV/c electron, and typical TLC parameters, this angle is about 70 mrad. Thus even with a crossing angle of this order, significant numbers of electrons will have even larger

angles, and may collide with the magnets. It is, however, possible (15,32) to devise magnetic fields that trap these low-energy pair electrons and funnel them out of the experimental area. But the fields must be present in the intersection, and thus in the detector, region. This will require careful design.

### 3. FINAL FOCUS

#### 3.1 Conventional Focusing

A final focus system is required to generate the small spot sizes needed to obtain a good luminosity. If a simple triplet or doublet of quadrupoles is used, with no chromatic correction, then the minimum  $\beta_{x,y}^*$  obtainable with a lens system, that will accept an angular divergences of  $\hat{\theta}_{x,y}$ , are given (33) by:

$$\beta_{x,y}^* = T_{x,y} \frac{E/e}{c} \frac{\hat{\theta}_{x,y}}{B^*} \delta_p^2 \quad . \quad 32.$$

where  $E/e$  is the beam energy in electron volts,  $c$  is the velocity of light,  $B^*$  is the maximum quadrupole pole tip field in Tesla,  $\delta_p$  is the half momentum-spread  $dp/p$ , and  $T_{x,y}$  are constants that depend on the details of the lens system. For two designs by Brown (34):

|       | <u>Triplet</u> | <u>Doublet</u> |
|-------|----------------|----------------|
| $T_x$ | 12.7           | 25.9           |
| $T_y$ | 9.47           | 2.2            |

As expected, the triplet will give minimum  $\beta^*$ 's that are almost equal in the two directions, and is suitable for round beams. The doublet gives a larger  $\beta_x^*$ , but a four-times-smaller  $\beta_y^*$ , and is best for a flat beam.

The acceptance angles  $\hat{\theta}_{x,y}$  are determined, in the case of a zero angle crossing, by the maximum disruption angles derived in Sec. 2.4, with a safety multiplier of

about 3. For a finite angle crossing scheme, in which the disrupted beam does not pass through the quadrupoles, the acceptance angles must be some factor  $S_\theta$  (e.g.,  $\approx 10$ ) above the incoming beam rms divergence, i.e.,

$$\hat{\theta}_{x,y} = S_\theta \sqrt{\frac{\epsilon_n}{\beta^* \gamma}} \quad , \quad 33.$$

from which one obtains the relation  $\beta^* \propto \epsilon_n^{1/3}$ .

Chromatic correction can be generated by a transport system, prior to the final focus, in which sextupole magnets are introduced into regions in which there is significant chromatic dispersion. Particles with different momenta pass through these sextupoles at different horizontal positions and receive correspondingly different focusing forces, these being used to cancel the momentum dependence of the focusing elsewhere. The systems are complex (35), correction must be made separately in the two directions, and the higher-order aberrations of the sextupoles must be cancelled. But all this is done for the SLC and the  $\beta^*$  achieved is a factor  $S$  of about eight less than that given by Eq. 32, for a momentum spread of  $\pm 0.5\%$ . Brown (36) gives an approximate scaling law

$$S \approx \frac{S_o}{\delta_p} \quad ,$$

where  $S_o$  is, scaling from the SLC, approximately 0.04. Using this relation I had specified (33) a TLC final focus that called for a factor  $S$  of 27 for a momentum spread of  $\pm 0.15\%$ . This was comfortably achieved in a detailed design by Oide (37).

### 3.2 Synchrotron Radiation (Oide Limit)

Oide (38) has calculated the dilution of focusing that arises from the quantum fluctuations in synchrotron-radiation in the magnetic fields of the final focus lenses. He

finds that there is a minimum rms beam size that is obtainable for a given beam emittance, obtained at a particular  $\beta^*$ . A larger  $\beta^*$  produces a naturally larger spot, but a smaller  $\beta^*$ , because of greater synchrotron radiation also increases the spot size. The minimum size is

$$\sigma \approx 1.83 (r_e \lambda_e F)^{1/7} \epsilon_n^{5/7} , \quad 34.$$

and occurs when

$$\beta^* \approx 2.39 (r_e \lambda_e F)^{2/7} \epsilon_n^{3/7} , \quad 35.$$

where the function  $F$  depends on the details of the final focus design, has a typical value of about seven; and an absolute minimum for a long, weak monopole, of about 0.1. Since  $F$  appears to the power one-seventh, it has only a weak effect on the limit.

For a low-energy collider like the SLC this limit is not significant, but in TLC designs it can be relevant, and in multi-TeV designs it is the effective bound (see Sec. 7.4). The only way around this limit seems to be the use of adiabatic focusing in a focusing channel of gradually increasing strength, as proposed by Sessler (39) (see Sec. 3.4).

### 3.3 Focusing Magnets

The above designs use conventional iron or permanent magnet quadrupoles with pole tip fields of the order of 1.4 T. In the TLC case, with finite angle crossing, the aperture of these quadrupoles is very small (of the order of 0.5 mm). If all the dimensions of a conventional iron pole, copper conductor, and quadrupole are scaled down uniformly, then the current density in the conductor must rise. Thus one is forced either to use:

(a) long tapering poles, driven either by relatively large conventional copper conductor cross sections (40) [Figure 12(a)], or by larger permanent magnets [Figure 12(c)]; (b) permanent magnets [Figure 12(b)] (41); or (c) superconducting windings (40).

### 3.4 Exotic Focusing

Various ideas have been proposed to obtain smaller  $\beta^*$ 's than provided by conventional, chromatically corrected, quadrupole systems. It should be noted, however, that in many examples (see Secs. 7.3 and 7.4), the vertical  $\beta^*$  obtained is of the same order as the bunch length, and further reduction of the  $\beta^*$  would not increase the luminosity. We also saw that the focusing strength is limited by the synchrotron radiation in the focusing lenses, independent of the mechanism. At high energies, this limit can be reached with a conventional system. But stronger focusing could eliminate the need for chromatic correction, would remove some of the design constraints, would allow larger momentum acceptance, and would help in lower energy colliders like the SLC. Various ideas have been considered:

The use of quadrupoles without iron, with either superconducting, or pulsed currents, have been proposed by Skrinsky (42).

The use of a plasma, at or near the intersection point, was first proposed by Chen (43, 44). It has also been observed experimentally (45). In a relativistic charged particle beam, the electrostatic space charge fields are exactly cancelled by the self-pinch fields. However, if the beam enters a plasma, the electrons in the plasma can be expelled (for an electron beam), or sucked in (for a positron beam) so as to neutralize the space charge, and thus its defocusing field. One is left then with the uncanceled magnetic pinch field that focuses the beam. The focusing can be very strong indeed, but suffers from some severe difficulties:

1. The focusing fields are nonlinear and depend on the charge distribution of the beam. As a result, the plasma lens has to be placed very near to the intersection.
2. The axis of the focusing is the axis of the beam itself, and any misalignment of the beam is not reduced, as would be the case for a conventional lens;
3. For the above mechanism, the plasma density must be higher than that of the beam. In the SLC case, this requires a density of the order of  $5 \times 10^{18} \text{ cm}^{-3}$ , which would yield a background of a few events per bunch crossing, which may be unacceptable. For a TLC the plasma density would have to be about four orders-of-magnitude higher; it would be hard to generate, and would produce a hopeless background.

Some focusing is also obtained with a plasma density that is less than that of the beam (46). In this case, an electron beam will expel all the plasma electrons, leaving the uniform positive ions that will focus the beam. This effect requires a much lower density plasma, is linear, but still suffers from the increased tolerance problem. The positron beam will attract electrons into the beam, as in the dense plasma case, the focusing will not be linear.

The use of a graded plasma to adiabatically focus a beam has been studied by Sessler et al (39). It is found that providing the initial normalized emittance is less than a critical value ( $\epsilon_n^{crit} \approx 6.17 \times 10^{-6} \text{ m}$ ), then an adiabatic channel with the correct gradient will, even though the emittance grows, focus a beam down without limit. As in the conventional plasma focusing, the densities required for a 0.1 TeV SLC example are already serious. The plasma proposed in Ref. (39) for a TeV example, has a final plasma density of  $1.8 \times 10^{23} \text{ cm}^{-3}$  and would, once again, yield a certainly unacceptable background from beam-plasma collisions.

Another exotic scheme, "super disruption," was proposed by Leith & Palmer (47). In this idea, two bunches are accelerated and brought to the intersection. The first bunch, in each beam, is made larger than the second, and is used as a lens to focus the oncoming second bunch in the opposite beam. In principle, very small  $\beta^*$ 's can be achieved, but the focusing bunch has to have a population of the same order as the second focused bunch. It thus uses significant beam power and, if accelerated through the same acceleration structure, would generate wakefields that would perturb the second bunch. The focusing bunch could have a lower energy than the second bunch, and it could be accelerated in a different structure, but the critical alignment of the two bunches would then be hard to achieve. Also, this scheme would still be subject to the Oide limit.

A variant of super disruption would be to use bunches graded in size and density: larger at the front, smaller at the back. In this way, adiabatic focusing might be achieved, and the Oide limit circumvented. Unfortunately, long bunches with large disruption parameters  $D$  would be required. These would suffer from the kink instability mentioned above (Sec. 2.5), and would not be stable. It might, however, be possible to adiabatically focus a lower current, short, positron bunch (whose emittance and Oide limit would be determined by a damping ring) by passing it through a higher current long electron bunch from a lower emittance source.

## 4. LINAC

### 4.1 *Acceleration Structure*

Acceleration structures are usually of two basic types: standing wave, or traveling wave. The former are used for relatively long trains of bunches, the later for one or a few bunches. Since currently planned colliders use one, or at most a few, pulses, only traveling wave structures are being considered.

A standing wave structure fills exponentially, but always with some fraction of the rf power reflected. At a set field level, the bunch train is introduced, and a steady state can be established, where there is no further reflection, and energy is taken out of the cavity by the bunches at the same rate that it is made up by the rf. It is the initial reflection loss that makes such structures undesirable for colliders with few bunches. In addition, such structures are relatively complex and in such structures, the ratio of the peak fields in the cavities to the average acceleration  $\mathcal{E}_{pk}/\mathcal{E}_a$  is relatively high, and thus less acceleration can be obtained without breakdown.

In traveling wave structures, rf power is fed in at one end and, without reflection, passes down the structure at a relatively slow group velocity  $v_g$ . The bunch, or bunches are introduced when the rf has finally filled, or nearly filled, the full length of the section. If the rf pulse continues, power is inevitably lost out the far end, but this is of no disadvantage if the bunch train, being short, is then already gone, and the rf pulse is terminated.

There is a third possibility that would be efficient for long trains of pulses while maintaining the low peak-field-to-acceleration ratio. A continuous traveling wave structure could be fed by frequent directional couplers along its length. Filling would, as in a standing wave structure, involve some loss at the directional couplers, but a steady state could be established without such loss. This proposal has been described by Miller as a "linear resonant ring." It would perhaps be the preferred solution for longer trains of pulses in far future colliders where efficiency would be of the highest importance.

#### *4.2 Traveling Wave Structures*

The most commonly considered structures consist of a pipe with periodic constricting irises (or discs). The fields between successive irises advances by a phase which is

usually (for instance in the SLAC linac)  $2\pi/3$ .

The relative radius of the iris hole  $a$  to the wavelength  $\lambda$  is a critical parameter. It determines the group velocity  $v_g$ , the wakefields, the acceleration for a given power, and the ratio of peak fields to average acceleration.

The relation between group velocity and  $a/\lambda$  is plotted in Figure 13(a) and given approximately [obtained from a fit to calculations performed using the program TWAP (48)] by:

$$\beta_g = \frac{v_g}{c} \approx \exp \left\{ 3.1 - 2.4 \left( \frac{\lambda}{a} \right)^{1/2} - 0.9 \left( \frac{a}{\lambda} \right) \right\} . \quad 36.$$

The acceleration, for a given rf power is given by the elastance  $s_t$ , defined by

$$s_t = \frac{\mathcal{E}_a^2}{w_f} , \quad 37.$$

where  $\mathcal{E}_a$  is the average accelerating field in a section and  $w_f$  is the rf energy, assuming no losses, needed to generate that acceleration. This energy is not the same as that required ( $w$ ) to fully fill the section because, since the particle and fields are moving down the section at finite velocity, the length of the required field pulse is less than that of the section. Thus  $w_f = w/(1 - \beta_g)$ .

This corrected elastance is plotted in Figure 13(b) and given approximately by

$$s_t a^2 = s_{at} \approx 5.7 \times 10^{10} \beta_g^4 \quad (\text{VmC}^{-1}) . \quad 38.$$

When losses are included, the energy needed is increased. If the attenuation time of the rf pulse, passing down the section, is defined as  $t_0$ , then for a section of length

$L$  the energy required for the same average acceleration will, for a uniform structure, be:

$$w_{rf} = w_f \frac{\tau^2}{(1 - e^{-\tau})^2} \quad , \quad 39.$$

where

$$\tau = \frac{L}{t_0 v_g} = \frac{t}{t_0} \quad . \quad 40.$$

This attenuation time  $t_0$  is given approximately by [see Figure 13(c)]

$$t_0 = t/\tau \approx 45.5 \times 10^{-6} (1 + 1.25 \beta_g^{1.5}) \lambda^{1.5} \quad . \quad 41.$$

Finally we have the ratio of peak fields in the cavity to average acceleration [see Figure 13(d)]:

$$\frac{\mathcal{E}_{pk}}{\mathcal{E}_a} \approx 2 + 6.0 \beta_g \quad . \quad 42.$$

In order to maximize the acceleration for a given rf energy, we require a large elastance  $s_t$ , which from Eq. 38 is obtained with a small iris hole  $a$  and high group velocity  $\beta_g$ . Since, as we shall see in the next section, the wakefields are controlled primarily by the hole radius  $a$ , this parameter is not free. A high group velocity can be obtained (Eq. 36), but requires a small ratio of wavelength to iris hole  $\lambda/a$ . Since  $a$  is fixed, this implies going to shorter wavelengths. Three problems arise: (a) power supplies are harder to design at shorter wavelengths, (b) the attenuation time  $t_0$ , and thus the pulse length  $t$  is reduced (Eq. 41), implying a higher required peak power  $W_{peak}$  [see Figure 13(f)], and (c) the peak fields  $\mathcal{E}_{pk}$  in the structure are

increased. The increase in peak fields is offset, to some extent, by the higher fields before breakdown, obtainable with shorter wavelength and shorter pulses, but the rapid rise of  $\mathcal{E}_{pk}$ , above a group velocity of 0.3 c, sets a limit to how high a group velocity can be usefully used. The SLAC linac has  $a/\lambda \approx 0.2$  ( $\beta_g \approx 0.01$ ). Present designs for TeV colliders call for  $a/\lambda \approx 0.2$  ( $\beta_g \approx 0.1$ ).  $a/\lambda \approx 0.3$  may be appropriate for multi-TeV colliders.

Power efficiency is also improved by using a short relative fill time  $\tau$ , but this too increases the peak power requirement. In the SLC,  $\tau \approx 0.6$ , but in future colliders, where efficiency will have increasing importance,  $\tau \approx 0.45$  or 0.3 is more likely.

### 4.3 Transverse Wakefields

The transverse wakefield  $\mathcal{E}_t(z)$  is that average transverse field induced by the structure, at a distance  $z$  behind a charge  $Q$ , when that charge is displaced from the structure's axis by a distance  $y$ . A wake potential  $W_t$  is defined by

$$\mathcal{E}_t = W_t Q y \quad . \quad 43.$$

$W_t$  depends on the geometry of the cavities. For an iris loaded linac it is observed (49) to have an initial linear rise:

$$W_t(z \ll a) \approx 9.1 \times 10^{10} \frac{z}{a^{3.5} \lambda^{0.5}} \quad , \quad 44.$$

and a maximum, at  $z \approx a$  of

$$W_t(max.) \approx 3.5 \times 10^{10} \frac{1}{a^{2.2} \lambda^{0.8}} \quad . \quad 45.$$

A reasonable fit is given by

$$W_t \approx 1 / ([1/W_t(z \ll a)]^2 + [1/W_t(max.)]^2)^{1/2} \quad . \quad 46.$$

A typical wake, and the above fit, are shown in Figure 14.

The effect of the wake is, in the presence of a small initial bunch displacement  $y_{init}$  to cause a rise in the displacement of the tail of the bunch  $y_{final}$ . Using a two-particle model (50):

$$A_w = \frac{y_{final}}{y_{init}} \approx 1 + \frac{(Ne) \beta_{av} W_t(2\sigma_z)}{4(E/e)} z \quad , \quad 47.$$

where  $(Ne)$  is the charge of the bunch,  $\sigma_z$  is the rms bunch length,  $(E/e)$  is the beam energy in electron-volts, and  $z$  is the distance along the accelerator. If the displacement amplification  $A_w$  is less than about two, then this two-particle model is reasonably accurate. But when the amplification  $A_w$  is more than two, then a cumulative effect sets in and far larger final displacements are produced.

$\beta_{av}$ , in Eq. 47, is the average focusing strength along the accelerator. For a typical FODO quadrupole lattice, it is given approximately by

$$\beta_{av} = \left( \frac{\sin \mu}{\mu^2} \frac{(E/e)}{c} \frac{2a_q}{B_q F_q} \right)^{1/2} \quad , \quad 48.$$

where  $\mu$  is the phase advance per half-cell (typically  $45^\circ$ ),  $B_q$  is the pole tip field (typically  $\approx 1.4$  T),  $F_q$  is the fraction of linear length devoted to quadrupoles, and  $a_q$ , the aperture of the quad, is typically  $\approx 1.2 \times a$ , where  $a$  is the iris radius.

#### 4.4 BNS Damping

The transverse wake effects, described above, can be effectively controlled by BNS damping (51). An energy spread  $\Delta E$  is introduced between the front and back of the bunch where, in the two-bunch approximation:

$$2E\delta_p(s) \approx \Delta E(s) \approx \frac{e}{4} N W_t(2\sigma_z) \beta_{av}^2 \quad , \quad 49.$$

where  $N$  is the number of particles per bunch,  $W_t(z)$  is the wakefield potential, and  $\beta_{av}$  is the average focusing strength in the linac, which can be obtained from Eq. 48.

If the fraction of length  $F_q$  devoted to quadrupoles is constant, then  $\beta_{av} \propto E^{1/2}$ , the required fractional half-momentum spread  $\delta_p$  is a constant. If this momentum spread is maintained until the end of all acceleration, then it must be removed prior to the final focus by an acceleration section of length  $\ell_c$  operating at a phase advance of  $90^\circ$ . The length then required is

$$\ell_c = \frac{\delta_p E \lambda}{2\pi \mathcal{E}_a \sigma_z} \quad , \quad 50.$$

where  $p$  is the final momentum,  $\lambda$  the wavelength,  $\mathcal{E}_a$  the accelerating gradient and  $\sigma_z$  the rms bunch length. In practice the momentum spread would be removed prior to the end of acceleration, and less additional length would be required.

An alternative to introducing a momentum spread, and having to remove it, is to modulate the focusing strength with time. This can be done by the use of rf focusing, using either quadrupole rf structures, or accelerating cavities with elliptical irises. It has been studied in detail at CERN (52) and is proposed for the CLIC collider.

#### 4.5 Alignment Tolerances

A severe *tolerance* problem can come from the effects of the finite momentum spread and strong focusing needed for BNS damping. Two regimes can be distinguished (53), depending on the magnitude of the momentum dependent difference of the total phase advance  $\Delta\Phi$  of the transverse betatron oscillations. For  $\beta_{av} \propto E^{1/2}$ ,

$$\Delta\Phi = \sqrt{\delta_i \delta_f} \frac{2L}{\beta_f} \quad , \quad 51.$$

where  $\beta_f$  is the final  $\beta_{av}$ , and  $\delta_i$  and  $\delta_f$  are the initial and final rms fractional momentum spreads.

One can use this formula for momentum spreads arising either: (a) from the longitudinal emittance of the damping ring, or (b) from a momentum spread introduced for BNS damping. Although in the latter case, it gives an over-estimate of the  $\Delta\Phi$  because the wakefields act to reduce this phase difference.

1. **LARGE  $\Delta\Phi$**  If this phase difference is large compared to  $\pi/2$ , then the betatron oscillations become hopelessly mixed, and the effective emittance is determined by the magnitude of these oscillations. In this case, if significant emittance growth is to be avoided, we need an alignment tolerance  $\Delta y$  (to keep the beams position within 1  $\sigma$  of its size) of:

$$\Delta y < \sigma_y = \sqrt{\frac{\beta_s \epsilon_y}{\gamma}} \quad , \quad 52.$$

which is a severe requirement.

2. **SMALL  $\Delta\Phi$**  If the phase difference  $\Delta\Phi$  is less than about  $\pi/2$ , then the chromatic disturbance is similar to the dispersion of a dipole and the required rms alignment is given by (53):

$$\Delta y < \frac{\sigma_f}{\psi \delta_p} \sqrt{\frac{2}{N_q}} \quad , \quad 53.$$

where  $\sigma_f$  is the rms beam size at the full energy,  $\psi$  is the phase advance per lattice cell and  $N_q$ , is the number of quadrupoles,

$$N_q = \frac{4L}{\psi \sqrt{\beta_i \beta_f}} \quad , \quad 54.$$

where  $L$  is the length of the accelerator, and  $\beta_f$  is the focusing strength at the end.

This tolerance can be further relaxed (by a factor of the order of 4) if the resulting chromatic dispersion at the end of the linac is measured and corrected.

The value of  $\Delta\Phi$  depends critically on the loading  $\eta_1$ , which is the fraction of rf energy removed by a single bunch:

$$\eta_1 = \frac{N e s_t}{\mathcal{E}_a} \quad , \quad 55.$$

where  $s_t$  is the elastance from Eq. 38. The parameters being discussed at SLAC [see Sec. 7.3(G)] specify multiple bunches, light loading ( $\eta \approx 2.5\%$ ), little or no BNS damping, a small phase advance ( $\Delta\Phi \approx 1.5$ ), and alignment tolerances of the order of  $30 \mu$ . In contrast, the designs being discussed at CERN and Novosibirsk [see Secs. 7.3(C) and (E)] use only single bunches, have heavy loading ( $\eta \approx 8\%$ ), a lot of BNS damping,  $\Delta\Phi \gg 1$ , and tolerances of only a few microns. The SLAC approach would thus seem to be favored, but it does involve the very significant complication of multiple bunches.

#### 4.6 *Vibration Tolerances*

A tolerance of a different kind concerns the allowable random movement of components from pulse to pulse. Fixed misalignments can be corrected, but random movements cannot. The most severe restriction is on random motion of the linac focusing quadrupoles. For  $\psi = 90^\circ$  phase advance per cell, the tolerance required to keep the beams position within  $1\sigma$  of its size, is (53):

$$\Delta_y < \frac{2}{5} \frac{\sigma_o}{\sqrt{N_q}} \quad , \quad 56.$$

where  $N_q$  is the number of quadrupoles from Eq. 54.

In addition there will be tolerances on the random motion of elements in the final focus that are fractions of the final spot size.

Note that these tolerances must be reduced if there is significant multibunch kink instability (Sec. 2.5), and they may be relaxed due to the disruption self-alignment (Eq. 14).

These vibration tolerances are typically of the order of 10 nm for a 1 TeV collider, and as small as 1 nm for a 10 TeV collider. These may seem severe, but studies (54) of typical natural and man-made vibrations indicate that, providing low-frequency motion is corrected, they should not present an insuperable problem.

#### 4.7 Longitudinal Wakes

The *longitudinal wake* is defined by the average accelerating field  $\mathcal{E}_\ell$  seen by a particle traveling at a distance  $z$  behind a charge  $Q$ , where

$$\mathcal{E}_\ell = W_\ell(z)Q \quad .$$

At very short distances, it tends towards a constant that is dependent only (55) on the iris aperture  $a$ :

$$W_\ell(z \ll a) \approx 3.4 \times 10^{10} \frac{1}{a^2} \quad . \quad 57.$$

For distances of length of the order of  $a$  one finds (49):

$$W_\ell(z \approx a) = 1.23 \times 10^{10} \left(\frac{1}{z}\right)^{1/2} \frac{1}{a} \left(\frac{1}{\lambda}\right)^{1/2} \quad . \quad 58.$$

For intermediate values of  $z$ , a reasonable fit to the SLAC case is obtained (see Figure 15):

$$W_\ell(z) = \left( \frac{1}{[W_\ell(z \ll a)]^2 + [W_\ell(z \approx a)]^2} \right)^{1/2} \quad . \quad 59.$$

The acceleration  $\mathcal{E}_{net}$ , including the time-dependent wake effects and the rf time variation of accelerating field, is given by:

$$\mathcal{E}_{net} = \mathcal{E}_a \cos(\Phi + \omega z) - \int_0^{\infty} \frac{W_\ell(\zeta)}{\sqrt{\pi} \sigma_z} \exp\left\{-\frac{(z - \zeta)^2}{2 \sigma_z}\right\} d\zeta \quad . \quad 60.$$

where  $\omega$  is the rf frequency. These effects are relatively complex:

1. There is an average energy loss of the bunch (zeroth order).
2. There is a greater loss to the back of the bunch compared with the front (first order), that can be corrected by a suitable choice of rf phase  $\Phi$ .
3. If the bunch is long there is a significant second-order term, with the energies at the front and back being less than the center. This is, at least to some extent, compensated by the time variation of the accelerating field.
4. There is a third-order term that arises if the bunch is other than uniform in current density, e.g., Gaussian.

Figure 16 shows the wakefield-generated momentum spread generated in a Gaussian bunch passing through a SLAC-like structure.

It is possible, in principle, to correct these effects to a high order, for long bunches, but the tight constraint on the charge distribution in the bunch may be hard to maintain. For shorter bunches and Gaussian charge distribution, the fractional rms momentum spread  $\delta_p$ , after correction, is given very approximately by

$$\delta_p \approx \left(\frac{1}{5}\right) \frac{n e}{2 \mathcal{E}_a} W(\sigma_z) \quad . \quad 61.$$

#### 4.8 *Multibunch Effects*

The use of multiple but smaller bunches, instead of a single but larger bunch allows easier tolerances, higher efficiency for converting rf to beam energy, and resulting higher luminosities. Unfortunately, with conventional accelerating structures, the required parameters are such that the long-term transverse wakefields left by the earlier bunches cause unacceptable transverse displacement of later bunches; a process known as "beam breakup." In a traveling wave structure with  $a/\lambda \geq 0.2$ , only one dominant transverse mode causes this breakup. If one chooses a bunch spacing such that successive bunches always fall on a zero crossing of this mode then, in principle, the breakup would be eliminated. In practice, however, the tolerances on bunch spacing required are unrealistic, and the problem remains.

A solution, proposed by Palmer (56) is to design cavities with attached damping waveguides that would damp the unwanted transverse modes so strongly that negligible cumulative multibunch beam breakup would occur; or at least to damp them strongly enough that the tolerances on bunch spacing are not unreasonable. Thompson & Ruth (57) have shown that with a  $Q$  of 20,  $N = 1.75 \times 10^{10}$  particles per bunch, and 10 bunches spaced 10.5 cycles apart, then the required precision of bunch spacing is 0.5% for a 40% increase in displacement of the last bunch: a reasonable requirement to meet.

Palmer's structure is relatively complicated (see Figure 17), and involves slots in the irises. Models have been built at BNL, SLAC and at KEK, and a measured  $Q$ 's, for the dominant mode, of less than 15 have been observed. Calculations (58) indicate that the real  $Q$  is of the order of 9, which is more than adequate. More recently Kroll & Farcas (59), independently, have studied damped cavities without slotted irises. These too may be adequate, although some loss of elastance is involved.

Wakefield problems can also arise in the damping rings, but these too can probably be solved with the help of damped accelerating cavities (57).

There can also be problems in the damping rings, when the bunch-length-to-bunch-spacing ratio gets too small. This tends to arise if the structure wavelength is small, as is desirable from stored energy considerations. A solution may be to compress the bunch spacing in the damping ring, just prior to extraction.

Another problem with the use of multiple bunches is the difficulty of assuring that the energy of all bunches be the same. This is natural in a standing wave structure, but not in a traveling wave structure. The problem can be solved by introducing the first bunch before the structure is full. The field lost to the acceleration is then corrected by the greater length of acceleration seen by later bunches. Ruth (57) has shown that this method can give good correction so long as the number of bunches  $n_m$  is less than about  $0.25/\eta_1$ , where  $\eta_1$  is the loading as defined by Eq. 55. The required bunch spacing  $\Delta z$ , increased structure length  $L_n$ , the corresponding increased rf pulse length  $t_n$ , and thus the increase in rf energy  $J_n$ , are given by

$$\left(1 + \frac{n_m \Delta z}{t/c}\right) = \frac{L_n}{L} = \frac{t_n}{t} = \frac{J_n}{J} \approx \sqrt{n_m \eta_1} \quad . \quad 62.$$

#### 4.9 Field Limits

Field limits in small standing wave structures have been investigated by Wang & Loew (60). They find maximum surface fields, for pulse lengths between 1.5 and 3.8  $\mu\text{sec}$ , given by

$$\mathcal{E}_s \approx 195 [f(\text{GHz})]^{1/2} \text{ MeV/m} \quad . \quad 63.$$

The pulse duration dependence of the breakdown field has been quoted (57) as

$$\mathcal{E}_s \propto [t]^{1/4} \quad , \quad 64.$$

although a somewhat lower dependence was seen in Ref. 63. For very short pulses, consisting of only one-half of the cycle, fields as high as 1500 MeV/m have been observed, without breakdown (61); so some dependence continues up to very high fields. Combining Eq. 64 with Eq. 63, and the frequency dependence of the filling time from Eq. 41, yields the scaling law  $\mathcal{E}_s \propto f^{7/8}$ .

As the frequency rises, so the breakdown field rises until the surface heating limit is reached. Surface heating has been shown (62) to be independent of frequency but proportional, initially, to the fourth root of the number of cycles of the pulse. If a maximum temperature is set from either melting, or fatigue (63) considerations, then a new field limit is derived that rises as the one-eighth power of frequency (assuming the pulse length is proportional to the fill time). These limits are shown in Figure 3.

## 5. RF POWER SUPPLY

### 5.1 Introduction

To drive the accelerating structures, and not use excessive wall power, the supplies must have an efficiency as high as possible. In addition, the phase and amplitude must be controlled to about one part in a thousand. The SLC is powered by 3 GHz klystrons delivering 50 MW pulses at about 50% efficiency. Future colliders will require shorter wavelengths and much higher peak powers. For instance, for 100 MeV/m accelerating gradient, using 12 GHz, one would require about 250 MW for every meter of linac. The best currently designed sources meeting the amplitude and phase stability requirements are 100 MW klystrons designed at SLAC (64) and at Toshiba (65). Both of these operate at a voltage of approximately 400 KV, a current of 500 A, and 50% beam-to-rf efficiency. To power a 100 MeV/m linac, one such tube and modulator would be required every 40 cm. This would be very expensive, and one should consider alternatives.

Most conventional supplies, like the klystron [Figure 18(a)], generate a relatively high current beam from a thermionic cathode and accelerate it in a pulsed high-voltage gap. The beam is bunched in some way, and then decelerated in an output cavity, to extract rf power. Gain may be provided by a sequence of idler cavities. The bunching is usually produced by an rf-driven cavity and drift distance, but in a lasertron (66) [Figure 18(b)] the bunching is generated at a photocathode, by illuminating it with pulsed light. In the case of the Gyrocon (67) the bunching is replaced by rf-induced transverse deflections, but the principle is the same.

In any such device employing a round beam, it is found that the efficiency, from space charge considerations, is related (see Figure 19) to the perveance  $P_v$  defined by:

$$P_v = \frac{I(A)}{V^{3/2} (\text{Volts}^{3/2})} \quad , \quad 65.$$

where the beam energy is  $eV$ , the current  $I$ , and thus the output power is  $V \times I$ . If the efficiency is to be maintained, the output power is then proportional to  $V^{5/2}$ .

To raise the power, there are three options: (a) raise the voltage  $V$ ; (b) use a ring beam, flat beam, or multiple beams, to avoid the space charge problems that limit the perveance; and (c) use a longer duration of rf pulse and subsequently compress it. I will consider them in turn.

## 5.2 Very High Voltage "Relativistic" Beams

It would be difficult, using the pulse transformers common to klystrons, to significantly raise an anode voltage. Instead, acceleration techniques are proposed to raise the driver beam energy [Figure 18(c)]. Bunching can be performed longitudinally at lower energy, or magnetic bunching or chopping can be performed at full energy. The efficiency could be improved if the used beam, instead of being dumped, were

reaccelerated and used again and again. This is the "Two-Beam Accelerator" [Figure 18(d)] concept proposed by Sessler. Two different acceleration methods have been considered:

1. **INDUCTION LINAC DRIVEN** Sessler et al (68) used a beam from a 50 MeV induction accelerator to drive a Free Electron Laser (FEL), and generated 1.8 GW of 30 GHz rf with a beam-to-rf efficiency of 50%. Its application to a TeV collider has also been studied (69).

More recently a much lower energy beam, also from an induction linac, was used to drive an output cavity (70). Power of 0.5 GW was obtained at 11.4 GHz, again with a beam-to-rf efficiency of approximately 50%. These are encouraging, but there are difficulties:

- (a) The higher voltage implies intense x-ray production, requiring significant shielding, and probably forcing the location of such klystrons in the accelerator tunnel rather than in a gallery.
- (b) Induction linacs are expensive, per unit of energy, unless the drive current is very high (e.g.,  $\sim 10\text{K A}$ ). But such high currents require even higher beam energies.
- (c) There can be problems with transverse stability, and phase stability, of the required very high current beams.

2. **SUPERCONDUCTING LINAC DRIVEN** The use of a superconducting linac to drive the relativistic beam has been studied at CERN (8). It is attractive because the efficiency of both the acceleration cavities, and the low-power c.w. klystrons used to fill them, could be very high. Low-frequency cavities (e.g., 300 MHz) would be used to store the needed energy, and the cavity apertures would thus be large and not cause wakefields and beam breakup. The difficulty

is that the cost per unit of stored energy, at this time, is very high. As a result, the CERN group has been forced to consider only a very high frequency main accelerator (30 GHz) which, because of its small irises, has large wakefields, requires strong BNS damping and very stringent alignment tolerances. In addition, the need for significant power to cryogenically cool the cavity losses, leads to a less than ideal overall efficiency ( $\approx 25\%$ ). If the accelerating fields sustained by the superconducting cavities could be raised, and the losses reduced, this could become a very good solution.

### 5.3 *Wide or Multibeam Devices*

The space charge considerations that give rise to the dependence of efficiency on perveance (Figure 19), do not apply for a sheet beam. The relevant parameter then is the perveance per square cross section. If the sheet beam is wide compared to its thickness and if it flows near to a metal surface then the power can be raised roughly in proportion to this ratio. The sheet may be flat or in a ring.

Ring beams are employed in Gyroklystrons, and at the University of Maryland a 30 MW tube is under development (71).

A permanent magnet wiggler focused sheet beam klystron has been proposed by Miller & Herrmannsfeldt (72) that, if 1 m long, would give 300 MW at 11.4 GHz with 50% efficiency. In such devices there is a danger of feedback from the output to the input cavity of transversely polarized rf.

A proposal for a linear lasertron has been made by Palmer (73) and for a linear, controlled field emission "gigatron," by McIntyre (74). These devices would not suffer from the feedback problem, and could give high efficiency and power. But the economics of the laser driven cathode are questionable, and the technology of controlled field emission has yet to be demonstrated in a high power tube.

The use of multiple, or "cluster," beams, is actually quite old (75), but has been revived, combined with the use of magnetron type immersed field guns [Figure 18(e)], by Palmer & Herrmannsfeldt (76). The advantage of such devices is that the low perveance per beam, or element of beam, allows the possibility of very high efficiency. In the cluster klystron case, for instance, with a perveance of  $0.4 \times 10^{-6}$  per channel, an efficiency of over 70% was simulated. In addition very high powers are available: 42 beams, each operating at 28 MW would give over a GW. The main problem here is the need to develop long life, very high current density ( $\approx 40$  A/m<sup>2</sup>), thermionic cathodes.

Another device that has a nonround beam is a Cross Field Amplifier (77) [Figure 18(f)]. Magnetrons are well known as low-cost rf sources, but are not amplifiers, and thus do not give the needed phase and amplitude control. This problem is solved in a CFA by the introduction of rf absorption in one sector of the magnetron. Such devices do not now operate at high power levels, but R & D is ongoing at SLAC.

#### *5.4 Rf Pulse Compression*

The output of the SLAC 3 GHz klystrons is pulse compressed by a factor of 3, with  $\approx 50\%$  efficiency, using a system known as SLED (Stanford Linac Energy Doubler). The idea is shown in [Figure 20(a)]. Initially power is fed into two cavities via a 3 Db hybrid (or magic T). During filling, the phase of the power leaking from the cavity approximately cancels that reflected at the cavity entrance, and little is lost. When the cavities are full, the phase of the klystron is reversed. Now the two phases add and the power leaves via the hybrid to the accelerator. Unfortunately the output pulses are not flat, the efficiency is not high and the maximum power gain is only of the order of 3.

Another idea has been proposed by Farcas (78), known as Binary Pulse Compression [see Figure 20(b)], that avoids the above disadvantages. The output pulses are flat, the efficiency, in the absence of losses, is 100%, and the compression can be repeated two or more times to give any desired power gain. But it is relatively complicated and involves relatively large lengths of waveguide.

In the recently proposed (79) super-SLED [see Figure 20(c)], the cavities of the original SLED are replaced by waveguides. In this case the output pulses are again flat, the gain per stage is 3, at over 90% efficiency. The gain can be more, at lower efficiencies, and the compression can be repeated. Its efficiency is not as good as the binary scheme, but its greater simplicity is attractive.

Rf pulse compression would be an effective tool in raising the available rf peak power from any high voltage gap driven source, such as a klystron, gyrotron, magnetron, etc., providing they are able to deliver the longer pulse. It is less useful in combination with an accelerator driven relativistic klystron or FEL, because the acceleration device, be it induction unit or superconducting cavity, is limited in total energy. It cannot give a longer pulse without lowering the available power.

### *5.5 Electrical Supply and Efficiency*

Most klystrons, and similar devices, are driven through a pulse transformer from a thyatron-switched pulse forming network, known as a "modulator." The cost of these modulators is typically about a factor of 3 greater than that of the klystrons they drive. The induction units in an induction driven relativistic klystron are powered by "magnetic amplifiers." These are passive magnetic devices that, by using the saturation of iron (or metglass), progressively shorten a pulse and raise its amplitude. The magnetic amplifiers are, in turn, driven by a modulator. As in the case of a conventional klystron, this power source, combined with the induction core is far more

expensive than the klystron cavities or FEL undulators that they drive. Similarly, in the CERN two-beam scheme, the dominant cost is of the superconducting cavities, which are, in that case, the source of drive energy. Thus we see that the power supply cost can, and in most cases does, dominate the cost per Joule of rf energy.

The efficiency of the power supplies is also a problem. Because it is hard to obtain very rapid rise and fall times, and because we can, in general, only use the flat top of the pulse (e.g., for the multipulse energy correction), the efficiency of conventional modulators is only about 60%. If magnetic amplifiers are used to give the needed short pulses, then the efficiency is even lower. This might imply an advantage for using the longer pulses and rf compression, but then the inefficiencies of the compression system (efficiency  $\approx 70\%$ ) must be included. In either case the overall efficiency for most cases (where beam to rf efficiency is  $\approx 50\%$ ) will be about 20%.

The only devices that would seem to avoid these problems are those that can in themselves switch the current. Such devices could be supplied from a dc source via a high voltage cable or delay line. The power supply efficiency would be high ( $\approx 90\%$ ), the rise and fall time almost instantaneous, and the

low. This was proposed first for the lasertron (74), and could also be used with a controlled field emission gigatron, a grid controlled klystron, possibly by a cross field amplifier (whose current should not flow until the rf is applied), and with a mod-anode controlled device such as the "cluster klystron" (76). The greatest difficulty in applying this idea is the need for the device to permanently withstand the full high voltage (actually it must withstand more than the operating voltage) without breakdown between pulses. The cluster klystron with its wide acceleration gaps is perhaps the best suited to this approach. In this case, since the beam to rf efficiency should be of the order of 70%, the overall efficiency might be as high as 60%.

## 6. ELECTRON AND POSITRON SOURCES

### 6.1 *Electron Source*

Electrons are, in the SLAC collider, obtained from a grid controlled thermionic cathode. They are then bunched, accelerated, injected into a damping ring, bunched again, and injected into the main linac. Partially polarized electrons can be obtained from suitable photocathodes illuminated by polarized light (80).

Electrons of great brightness ( $I/\epsilon_n^2$ ) can be obtained from photocathodes (81), so that one might contemplate eliminating the electron damping ring. But without some special intersection geometry, little advantage in luminosity is to be expected if the positron emittance remains limited by its damping ring.

Bunching in the SLC is performed by a brief acceleration with a phase  $\Phi$  to introduce a momentum spread between front and back; followed by a chromatically corrected bend with finite negative longitudinal dispersion (so that higher momentum particles take longer than lower momentum ones). For a future collider requiring bunch lengths of the order of  $100 \mu$ , two such stages of bunch compression would be required (82).

### 6.2 *Positron Source*

Positrons in the SLC are obtained by bombarding a moving thick metal target with electrons of 15 GeV energy. After capture and reinjection into the linac, about one positron remains for each electron on target. The only serious problem in this method is the heating of the metal target. Luckily the specifications of future higher energy colliders do not call for much higher average currents of positrons than in the SLC, and thus do not seem to pose a serious problem.

An alternative method of positron production is proposed by the Novosibirsk study (6), in which the used electron or positron beam is passed down a long magnetic

undulator. Polarized photons are generated, and these are brought onto a thin metal target, where pairs of polarized electrons and positrons are made. The method, to be effective, needs higher energy particles than the target method, but appears to be the only way to obtain polarized positrons, if these are desired. In either method, the emittance of the positrons is relatively large and a damping ring is essential.

### 6.3 Damping Ring

The transverse emittance is lowered in a damping ring by the emission of synchrotron radiation which lowers both longitudinal and transverse momentum. The longitudinal momentum lost is made up by the rf cavities, without adding any in the transverse directions. The process continues until as much transverse momentum is being added by the statistical fluctuations in the photon emission, as is being removed by the damping process.

We can obtain a qualitative understanding of the parameters of the damping rings by calculating the performance of an idealized ring, in which it is assumed that the focusing strength  $\beta$  is constant.

Since wigglers in a damping ring improve both the equilibrium emittance and the damping time, they should be included. For simplicity we can consider rings of the continuous wiggler type (83). All bending magnets in the ring consist of at least one inward bend and one outward. The average bending field  $\langle B_d \rangle = \xi B_D$ , where  $B_d$  is the local fields in the magnets, and  $\xi$  is a factor less than 1 and  $F_m$  is the fraction of the ring circumference filled by dipoles.

The emittances both vertical and horizontal are damped by the emission of synchrotron radiation with a time constant (84):

$$\tau_{x,y} \approx \frac{8.3}{J_{x,y}} \frac{1}{B_D^2 \gamma F_m} \text{ (mks)} \quad , \quad 66.$$

where  $J_x, J_y$  are the partition functions, usually  $J_x \approx J_y \approx 1$ .

If there is no mixing between the horizontal ( $x$ ) and vertical ( $y$ ) oscillations, then the vertical emittance will damp continuously. But the horizontal emittance will settle at an equilibrium value. At high energies this value is set by the effect of quantum fluctuations:

$$\epsilon_{nx}(\text{quantum}) \approx \frac{2.2 \times 10^{-10}}{J_x} \beta_x B_D \frac{\gamma^2}{Q_x^2}, \quad 67.$$

where  $\beta_x$  is the average focusing strength ( $\beta_x = R/Q_x$ ),  $R$  is the average radius of the ring, and  $Q_x$  is the tune of the ring.

If the repetition rate of the collider is very high, the choice of operating energy  $\gamma$  may be determined by the required damping time  $\tau$ , in which case the equilibrium emittance  $\epsilon_n \propto N/(B_D^5 \tau^3)$ . But for a high-energy collider, with finite wall power consumption, the repetition rate cannot be so high. In addition, serial damping rings could be used: the former having a fast damping time but higher equilibrium emittance, and the latter used only for a short duration to bring the emittance down to the required value. In this case, the damping time can be neglected and the energy lowered until intrabeam scattering becomes significant. This scattering of particles of different momenta within the bunch sets a minimum emittance (85):

$$\epsilon_{nx}(\text{intrabeam}) \approx \frac{1.2 \times 10^{-10}}{B_D} \left[ \frac{N}{\epsilon_z \gamma F_m Q_x \zeta J_x} \left( \frac{\beta_x}{\beta_y} \right)^{1/2} \right]^{1/2}, \quad 68.$$

where  $\epsilon_z = \gamma (dp/p) \sigma_z$  and  $\zeta$  is the ratio of vertical to horizontal emittances. We note from the different  $\gamma$  dependencies of the quantum and intrabeam emittances, that there must be a minimum emittance  $\epsilon_{nx}(\text{min.})$  (see Figure 21) which is found to be

$$\epsilon_{nx}(\text{min.}) \approx 1.4 \epsilon_{nx}(\text{quantum, at } \gamma = \gamma_0) . \quad 69.$$

where  $\gamma_o$ , when given as a function of the required emittance  $\epsilon_{nx}$  is:

$$\gamma_o \approx 2.1 \times 10^{-7} \left[ \frac{N (\beta_y/\beta_x)^{1/2}}{\epsilon_{zn} B_D^{2.5} \zeta J_x^{1/2} F_m k_1^{1/2}} \right]^{4/9} \left( \frac{1}{\epsilon_{nx}} \right)^{2/3}, \quad 70.$$

and  $k_1 = \beta_x/\gamma^{1/2}$ . Substitution of this into Eq. 67 gives the required tune  $Q_x$ . This tune may be limited by various factors: the acceptance of the ring, the bunch longitudinal instability, or tolerance requirements. In current designs, with  $N \approx 10^{10}$  it seems to be the impedance requirement that is most critical:

$$\frac{Z}{n_z} \leq \frac{(2\pi)^{3/2} \sigma_z (E/e) \alpha \delta_p^2}{ceN}, \quad 71.$$

where  $n_z = R/\sigma_z$ , the momentum compaction  $\alpha \approx 1/Q_x^2$ , and  $\delta_p$  is the fractional momentum spread. If this is substituted into Eqs. 70 and 67, then one finds that the minimum emittance is

$$\epsilon \propto \frac{N^{0.62}}{B_D^{1.63}}. \quad 72.$$

For very low  $N$ , however, the limit will probably be set by the acceptance:

$$\hat{\epsilon}_n \approx 6 \times 10^{-4} \gamma R \frac{Q_y}{Q_x^4}, \quad 73.$$

Damping rings have been designed for future colliders both at SLAC (86) and CERN (87) which have performance in quite good agreement with these approximate formulae.

We note that in all cases the emittance is reduced by a high damping field  $B_D$ , a large fraction of the ring full of such magnets  $F_D$ , small strong quadrupoles  $k_1$ , a large partition function  $J_x$ , and a large longitudinal emittance  $\epsilon_{nz}$ .

The damping field  $B_D$  is usually limited by iron saturation, but could be raised by the use of a superconducting wiggler. Superconducting quadrupoles to raise  $k_1$  could also be contemplated, but the gain is not so large. The partition function  $J_x$  can be raised by the use of "Robinson" wigglers which have strong field gradients such that higher momentum particles, that move in a straighter orbit, see lower bending fields. As  $J_x$  rises,  $J_z$  falls while keeping  $J_x + J_y + J_z = 4$ . This fall in  $J_z$  is helpful since it raises the equilibrium momentum spread  $\delta_p$  and eases the impedance requirement of Eq. 71. Raising the longitudinal emittance  $\epsilon_{nz}$  is also facilitated by the increase in  $\delta_p$ , since the bunch length is constrained by practicalities of the rf and by quantum lifetime if there are multiple bunches.

Other useful relations are:

$$\text{Momentum spread } \frac{\sigma_p}{p} \approx \frac{2}{J_z} 1.1 \times 10^{-5} (\gamma B)^{1/2} \quad , \quad 74.$$

$$\text{Dispersion } \eta \approx \frac{\beta_x^2}{R} \quad , \quad 75.$$

$$\text{rf volts/turn } U \approx 3.2 \times 10^6 \frac{\gamma}{h} \left( \frac{R}{Q_x} \frac{(\sigma_p/p)}{\sigma_z} \right)^2 \quad , \quad 76.$$

where  $h$  is the harmonic number of the rf,

$$\text{energy loss/turn } V = 5.78 \times 10^{-9} \frac{\gamma^4}{\alpha^2 R F_m} \quad . \quad 77.$$

## 7. EXAMPLES

### 7.1 Introduction

The design of linear colliders is a complex problem because of the interdependence of the critical parameters. The situation is illustrated by Figure 22 and has been discussed in more detail in Ref. (33). Changing the number of particles per bunch effects the damping ring design and thus the emittance; it effects the wakefields in the linac and thus the momentum spread; the momentum spread effects the final focus design and thus the final  $\beta^*$ ; but the emittance change also effects the final focus design; and all these come together to determine the luminosity, disruption and beamstrahlung at the intersection. Changing the bunch length, or almost any other parameter, has a similar chain reaction. Dealing with this problem by simple scaling laws is very difficult because one does not know which parameter is going to be critical and thus which should be held constant. One can only find solutions by a process of search and iteration.

The following examples (Tables 1-3) were found with the aid of a computer program, using the approximate formulae given in the earlier sections of this review. They are each self-consistent, and, given the constraints in each case, optimized for maximum luminosity.

### 7.2 Assumptions

1. RATIO OF HORIZONTAL TO VERTICAL EMITTANCES I have assumed relatively large ratios of horizontal to vertical emittances in the damping rings. An asymmetric emittance is natural in a damping ring and comes with essentially no price. It easily allows the generation of a flat beam profile to minimize beamstrahlung, without loss of luminosity.

2. RATIO OF HORIZONTAL TO VERTICAL BETAS    Greater luminosity is obtained with smaller ratios of the betas; but the beamstrahlung rises, and has, in these examples, been limited to a value of  $\delta \leq 0.3$ . This ratio can also be used to control the beamstrahlung  $\Upsilon$  parameter, and to allow finite angle crossing without luminosity loss.
3. DAMPING RING    Wiggler damping rings are assumed. The energies are chosen to make the contributions from intrabeam scattering and quantum fluctuations the same. The ring diameters are then chosen to give a longitudinal impedance requirement of  $Z/n = 0.5 \Omega$ . The wiggler fields are, in most cases, 2 T, but is raised to 4 T (superconducting) for the 10 TeV case. The quadrupole apertures are 12 mm and pole tip fields, 1.4 T. The partition functions are, in most cases, normal,  $\beta_y/\beta_x = 4$ , and the phase advance per cell is  $65^\circ$ .
4. QUADRUPOLE DOUBLET FINAL FOCUS    Conventional, chromatically corrected quadrupole-doublet final focus is assumed. The ratio of the assumed corrected  $\beta$  to a calculated uncorrected value is taken to be  $S = 0.04 \times dp/p$  (scaling law from Brown). The maximum pole tip field, in most cases, is assumed to be 1.4 T. The aperture is taken to be ten times the rms beam size.
5. ACCELERATING STRUCTURE    Conventional iris loaded accelerating structures are assumed. The iris radius, in most cases, is taken to be 0.2 times the wavelength. This gives a relatively high group velocity (0.08) and lower wakefields than for a SLAC-like structure (radius 0.1 times the wavelength). For the 5 and 10 TeV examples, it is raised to 0.25 and 0.3, respectively, to ease wakefields and resulting tolerances. The fill time for the structure is usually taken to be 0.45 times the attenuation time. In the 5 and 10 TeV cases, it is lowered to 0.3 for maximum efficiency.

6. LINAC FOCUSING Five percent of the linac length is assumed taken up with quadrupoles whose apertures are 1.26 times the structure irises and whose pole tip fields are 1.4 T.
7. NUMBER OF BUNCHES In all but the multi-TeV examples, a limit is set on the number of bunches such that not more than 25% of the total stored energy is extracted. This is consistent with the conventional traveling wave design. In the 5 and 10 TeV examples, this percentage is raised to 75%, on the assumption that a linear resonant ring design is adopted.
8. DILUTION No machine is perfect, so in designing it one must make allowances for the imperfections, whose effect will be to dilute various parameters. The following dilutions are assumed:

|  |       |
|--|-------|
| Emittance $z$ in buncher:                  | 1.4   |
| Emittance $x$ from kicker:                 | 1.4   |
| Particle transmission through buncher:     | 1/1.2 |
| Emittance $y$ in linac:                    | 1.4   |
| Particle transmission through final focus: | 1/1.2 |
| Emittance $xy$ in final focus:             | 1.2   |
| $\beta^* xy$ in final focus:               | 1.2   |

9. LONGITUDINAL EMITTANCE The longitudinal emittance is constrained by the need to restrict the momentum spread in the linac, and thus the range of phase advances and resultant alignment requirement. It is also restricted by rf voltage considerations in the damping ring. In some multibunch cases it is further restricted in order to keep a sufficiently small ratio of bunch length to bunch spacing in the damping ring.

10. ACCELERATING FIELDS From the machine physics point of view there seems no disadvantage in high accelerating fields. The optimized luminosity is little effected, the tolerances are easier and of course the length is less. The field used should thus be the highest possible consistent with breakdown and dark current considerations.

### 7.3 Philosophies

Depending on one's philosophy, one can come up with quite different collider designs. In order to illustrate this, I give (in Tables 1 and 2) eight different designs of a 0.5 TeV center-of-mass energy collider. Each is constrained to use the same wall power (70 MW) and the same rf source efficiency (20%). The designs vary in their having (a) single or multiple bunches, (b) head-on or finite angle collisions, (c) crab crossing or no crab crossing, (d) conventional (1.4 T pole tip field) final focus quadrupoles or exotic focusing (5 T), and (e) 11.4 GHz rf or 30 GHz rf.

The desired luminosity, to give 10,000 events per year of  $R$ , is  $2.5 \times 10^{33} \text{ cm}^{-2} \text{ sec}^{-1}$  (see Figure 5). As we will see, this is not so easy to obtain.

7.3.1 SINGLE BUNCH DESIGNS In all the single bunch cases, it is found that maximum luminosity is obtained when the number of particles per bunch is maximized. The loading  $\eta$  can be allowed to rise to between 8% and 12%, while great care is exercised to correct the momentum spread that comes from the longitudinal wakes. The transverse wakes are severe ( $C_w \gg 2$ ) and BNS damping is essential and strong (the required  $dk/k = 3\%$ ). This might best be applied by modulating the focusing strength rather than the momentum, but in either case, the differences in phase advances in the linac are large and the alignment tolerances severe (below  $2 \mu\text{m}$ ). The luminosities obtainable vary with the assumptions, but in no case can the aimed for  $2.5 \times 10^{33} \text{ cm}^{-2} \text{ sec}^{-1}$  be achieved.

In the following, the letters refer to the columns in Table 1.

(A) Head-on, conventional quadrupole, 11 GHz:

In this case, the quadrupole apertures have to accept the disrupted beam, and have, as a result, limited strength ( $\beta^* = 4.3$  mm). The maximum luminosity is only  $0.24 \times 10^{33}$  (1/10 the required value).

(B) Head-on, high field quadrupole, 11 GHz:

If an exotic quadrupole (pole tip field = 5 T) is employed, the focus strength can be increased ( $\beta^* = 1.9$  mm) and the luminosity is increased in proportion, to  $0.6 \times 10^{33}$  (1/4 that required).

(C) Flat beam, finite angle crossing, conventional quadrupole, 11 GHz:

This is the philosophy, but not the particular parameters, that has been pursued at Novosibirsk (7). A finite crossing angle is employed, that is much greater (by a factor of 25) than the disruption angles. The disrupted beam, instead of passing through the quadrupole aperture, now passes to one side of the quadrupole, and, as a result, the quadrupoles aperture is limited only by the incoming beam dimensions, which are far smaller. The apertures can be very small (0.6 mm), and the focusing strong ( $\beta_y^* = 0.13$  mm).

In order not to lose luminosity from this large crossing angle, a very wide flat (180 : 1) beam must be employed. The luminosity is increased, compared with case (A), but, because of the need for this very wide beam, the increase is not large (50%, to  $0.34 \times 10^{33}$ ). An advantage, however, is that the beamstrahlung is now relatively small ( $\delta = 8\%$ ).

We may note that in this case the vertical  $\beta^*$ , or "depth of focus," is already of the same order as the bunch length  $\sigma_z$  ( $\sigma_z/\beta_y^* = 0.7$ ). Further reduction in  $\beta^*$ , by the use of higher field quadrupoles, will thus not increase the luminosity.

(D) Crab crossing, conventional quadrupole, 11 GHz:

With crab crossing, we remove the constraint on the width of the beam, while retaining the advantage that the quadrupole does not have to contain the disrupted beam. One is free to reduce the width until the beamstrahlung  $\delta$  becomes unacceptable. With  $\delta = 0.3$  (obtained with a horizontal to vertical ratio of 39) one obtains a luminosity of  $1.2 \times 10^{33}$ , which seems the highest value obtainable with single bunches, at this radio frequency.

(E) Crab crossing, conventional quadrupole, 30 GHz:

This would be a possible philosophy for the CERN CLIC (8). The choice of the high operating frequency is dictated by the desire for a very low total rf energy (18 J, compared with 120 J for the 11 GHz cases).

Surprisingly, as the frequency is raised, the luminosity does not change much. The lower number of particles per bunch ( $1.7 \times 10^{10}$  instead of  $\approx 10^{11}$ ) is compensated by the lower emittance (1.9 mm mrad, instead of  $\approx 10$  mm mrad) that the damping ring can provide. As the number of particles per bunch falls, the beamstrahlung is suppressed. Rounder beams can be employed, the required ratio of emittances is not so severe (37 : 1, instead of 100 : 1). When all this is taken into account, a somewhat higher luminosity is obtained ( $1.8 \times 10^{33}$ ).

But the alignment tolerance is tighter (0.9  $\mu\text{m}$ , compared with 2  $\mu\text{m}$  for the 11 GHz cases). The tighter tolerance arises because the lower emittance, combined with the stronger focusing, gives a smaller beam size in the linac.

7.3.2 MULTIPLE BUNCH DESIGNS     If the problems with beam breakup can be solved by the use of damped cavities, then the whole optimization of the collider is changed. Instead of employing a few large bunches, greater luminosity is obtained using a larger number of small bunches. Not only is greater luminosity obtained, but

one finds that the momentum correction is now trivial, the BNS damping is weak, the differences in phase advance in the linac are less than 1.5 rad, and the alignment tolerances are much easier (20–30  $\mu\text{m}$ , instead of 1–2  $\mu\text{m}$ ).

I will consider four cases (the letters refer to the columns in Table 2):

(F) Flat beam finite angle crossing, conventional quadrupole, 11 GHz:

This is the philosophy discussed in my previous paper (33). As in example (C), the crossing angle is chosen to be 25 times the disruption angles, so that the used beam can pass outside the quadrupole aperture. A very flat beam (aspect ratio 180 : 1) is needed to avoid luminosity loss from the finite angle crossing. The finite crossing angle allows the multiple bunches to interact strongly only at the intersection point, but the long-range interactions do excite the kink instability (Sec. 2.5) resulting in an amplification of misalignments by the factor  $C_n$  of 1.4. A luminosity of  $1.4 \times 10^{33}$  is obtained (four times that obtained in the single bunch case), and the beamstrahlung energy loss  $\delta$  is only 3.9%. A possible problem with this design is the electron pair production (Sec. 2.7) that may generate an unacceptable experimental background.

(G) Crab crossing, conventional quadrupole, 11 GHz:

This is the philosophy now considered at SLAC. The crab crossing (Sec. 2.2) allows a large enough crossing angle to avoid background problems from electron pairs, and it allows any desired aspect ratio to be used. For maximum luminosity consistent with the requirement of beamstrahlung  $\delta < 0.3$ , the aspect ratio is 25 : 1, and a luminosity of  $5.8 \times 10^{33}$  is obtained (five times that obtained with the single bunch, and over twice that required). If other aspect ratios are chosen, both beamstrahlung and luminosity vary as shown in Figure 23. One must note, however, that points on this figure represent different damping ring

and final focus designs. With a fixed design optimized at one particular aspect ratio, the other aspect ratios will yield somewhat less luminosity.

From Figure 23, we see that very high luminosity appears possible for very high values of the beamstrahlung parameter  $\delta$ . Since  $\delta$  represents the fractional energy of loss of the beams, values above one need interpretation. They imply almost total conversion of the electron beams to real high-energy photons. The electron-positron luminosity is suppressed, but there remains a significant and interesting cross section for photon-photon interactions (88).

For the  $\delta = 0.3$  case, the bunch length is significantly less than the  $\beta_y^*$  ( $\sigma_z/\beta_y^* = 0.32$ ), so one might expect that the luminosity could be significantly improved by the use of higher field quadrupoles. This turns out not to be true. As the focusing strength is increased, the beamstrahlung is also increased, and a wider beam must be employed to control it. The net luminosity increase from the use of a 5 T (instead of 1.4 T) quadrupole is only 25%, which hardly seems worth it.

(H) Crab crossing, conventional quadrupole, 30 GHz:

This would be a possible philosophy for CERN to follow, if they wished to raise the luminosity and ease the tolerances, yet maintain the high frequency, and consequent low total rf energy. In order to keep the range of phase advances below 1.5 rad (so that the tolerances can be eased) one finds it necessary to use very small bunches ( $1.8 \times 10^9$  electrons). Twenty bunches can then be used, and a luminosity of  $4.1 \times 10^{33}$  is obtained. But the bunches are now spaced by only three cycles and the bunch-length-to-spacing ratio in the damping ring is 0.6, which would not be acceptable. Some scheme for compressing the bunches together, prior to extraction, would have to be used. Another problem is that

the damping time is rather long (4 msec) compared with the high repetition rate (900 Hz). A predamping ring would be essential.

It is clear that this case has not been fully optimized, but it illustrates the basic insensitivity of the luminosity to the wavelength used. However, tolerance and damping ring problems get worse for shorter wavelengths. Luminosity is also insensitive to the accelerating gradient. Tolerance and damping ring problems improve with higher gradients.

#### 7.4 Designs as a Function of Energy

At higher center-of-mass energies, for the same event rates, we require luminosities given approximately by  $L \approx 10^{34} E (\text{TeV})^2 \text{ cm}^{-2} \text{ sec}^{-1}$  (Sec. 1.6, and Figure 5). In Table 3 examples are given for four energies up to 10 TeV. These examples achieve these required energies and luminosities by using progressively higher gradients, lower wavelengths, higher wall power and increasing damping ring sophistication. In all cases, multiple bunches and crab crossing are assumed. In column (N), for comparison, the approximate parameters for the SLC, calculated in the same way, are also given.

The letters below refer to columns in Table 3.

(I) ILC, an intermediate 0.5 TeV linear collider:

This is essentially the same as example (G) above, except that a flatter beam (100 : 1), easier crab crossing requirements, and lower beamstrahlung (0.07), has been chosen.

(J) TLC, a 1 TeV collider:

It is assumed that a more advanced power source will allow the gradient to be raised to 150 MeV/m. No change in wavelength is assumed, and the repetition rate remains the same (120 Hz).

The four-times-higher luminosity ( $1 \times 10^{34}$ ) is obtained from: (a) an assumed improvement in the power source efficiency (from 20% to 40%); (b) a 40% increase in wall power (from 70 to 100 MW); and (c) by allowing the beamstrahlung  $\delta$  to rise to 0.3.

Care has been taken to keep the beamstrahlung quantum parameter  $\Upsilon$  at no more than 0.6, so that the coherent pair production is not a problem.

(K) 5TLC, a 5 TeV collider:

In order to avoid an excessive rise in the total rf stored energy, the wavelength is reduced to 12 mm. At this frequency breakdown and dark current should be less of a problem, so the accelerating field can be raised to 200 MeV/m.

The required 25-fold increase in luminosity (to  $2.5 \times 10^{35}$ ) is obtained by: (a) a further increase in assumed rf power source efficiency to 60% (e.g., by using uncompressed cluster klystrons); (b) assuming the use of a standing wave, or linear resonant ring structure (Sec. 4.1), with a bunch train running for 75% of the fill time; and (c) assuming a damping ring with Robinson Wigglers, so that the horizontal partition function is raised to 2.5 (and the longitudinal partition function lowered to 0.5).

One may note that in this example the vertical size of the beam at the intersection (0.2 nm) is essentially equal to the Oide limit (Sec. 3.2). No further reduction in size is possible without a further reduction in vertical emittance. Stronger quadrupoles will not help.

(L) 10TLC, a 10 TeV collider:

Once again the wavelength has been reduced (to 10 mm), and the accelerating gradient increased (to 300 MeV/m). A more drastic reduction of wavelength would lower the now very large stored energy (1.2 kJ), but the bunch spacing

then becomes small compared with the bunch length in the damping ring (now only a factor of 5, already requiring the use of higher harmonic rf). The possibility of compression of the bunch train before extraction would relieve this constraint, and needs to be studied.

No further improvement in rf efficiency or number of bunches seems realistic, so the required increase in luminosity can only come from a reduction in spot size. This, since one is at the Oide Limit, can only come from a reduction in the emittance. One needs a further improvement in the damping ring, and the only remaining possibility here is to raise the wiggler magnetic fields (to 4 T) by the use of superconducting magnets. Whether this is really practical is not clear. The wigglers have quite a short period, and must have strong field gradients to obtain the still needed modification of the partition functions.

This 10 TeV parameter set is clearly very speculative, but it is significant nevertheless. The luminosity calculated in a self-consistent way, with possible dilutions included, is nearly six orders-of-magnitude higher than that of the SLC [see column (N)].

### *7.5 Energies Above 10 TeV?*

Whether one can reach yet higher energies, and obtain the yet higher needed luminosities, will depend on:

1. Ever more sophisticated and lower emittance damping rings.
2. Learning to use the lower emittances and higher electron currents, that can, in principle, be obtained from various cathodes.
3. Finding novel ways to obtain super low emittance positrons.
4. Finding ways to avoid the Oide limit, such as the use of adiabatic channel focusing (Secs. 3.2 and 3.4).

5. Learning to handle the electron pair background.
6. Learning to meet the ever-tighter tolerance requirements.

Experience suggests that ways will be found, but much work will be required.

## 8. CONCLUSION

The Stanford Linear Collider is now operating at a center-of-mass energy of 0.1 TeV, with a substantial, and rising, luminosity. This machine has taught a great deal about many unforeseen difficulties, but it has demonstrated all the fundamental requirements.

The technology to build an "intermediate linear collider" with a center-of-mass energy of about 0.5 TeV, and luminosity  $10^{33} \text{ cm}^{-2} \text{ sec}^{-1}$ , seems now to be available. The physics seems understood, suitable model damped structures have been built and tested, damping rings and final focus systems have been designed. With the 100 MW x-band klystrons and super-SLED pulse compression, one seems to have at least one practical and sufficient power source. Much R&D is still required, but one has no reason to expect serious difficulties.

Colliders in the energy range of 1 to 2 TeV, to be economical, will require cheaper, more efficient, and higher power, rf sources than are currently available. Switchable, wide, or multibeam devices (Sec. 5.3) are good candidates. Upgrades of lower-energy "intermediate" machines, by replacing their power supplies or increasing their length, might be possible.

Higher-energy colliders can be conceived. The main problem in their design is the need for luminosities that rise as the square of the energies. On paper, the required luminosities can be reached even at center-of-mass energies to 10 TeV (an available energy significantly higher than that of the proton-proton Superconducting Super

Collider, now under construction). Linear colliders do therefore offer the hope of going beyond this machine, in years to come.

Much work must be done if this possibility is to be realized. It is interesting to note, however, that the required work is not on the development of new exotic high-gradient accelerating mechanisms. What is needed is the development of very low-emittance damping rings, sophisticated focusing, correction, monitoring and alignment, and very high-efficiency acceleration systems and power sources.

This work was supported by the Department of Energy under contracts DE-AC03-76SF00515 (SLAC) and DE-AC02-76C0016 (BNL).

*Literature Cited*

1. Tigner, M. *Nuovo Cimento* 37: 1228 (1965).
2. Amaldi, U. *Phys. Lett.* 61B: 313 (1976).
3. Balakin, V. E., Budker, G. I., Skrinski, A. N. Novosibirsk preprint 78-101 (1978). Pres. at *Int. Sem. on Prob. on High Energy and Controlled Nucl. Fusion, Novosibirsk (1978)*.
4. Augustin, J. E., et al. *Proc. ICFA Workshop on Poss. and Limit. of Acc. and Detectors, Fermilab, 1978*, pp. 87-105. Batavia: Fermilab (1979); Richter, B. *IEEE Trans. Nucl. Sci.* NS-26: 4261 (1979).
5. Richter, B. AATF/7913 (1979).
6. Richter, B. SLAC-PUB-5075; *Proc. Int. Conf. on High Energy Acc., Tsukuba, Japan, 1989*.
7. Balakin, V. E., Skrinsky A. N. *Proc. Int. Conf. on High Energy Acc., Tsukuba, Japan, 1989*.
8. Schnell, W. CERN-LEP-RF/86-06 and CERN-LEP-RF/86-27.
9. Palmer, R. B. *Part. Acc.* 11: 81 (1980).
10. Willis, W. *Proc. Workshop on Laser Acc. of Part., Malibu, CA, AIP Conf. Proc.* 130: 421 (1986).
11. Voss, G.-A., Weiland, T. DESY M-82-10 (1982); Voss, G.-A., Weiland, T. *Proc. ECFA-RAL Workshop, Oxford, 1982*, ECFA 82/68 and DESY 82-074 (1982).
12. Tajima, T., Dawson, J. M. *Phys. Rev. Lett.* 43: 267 (1979).
13. Chen, P., Huff, R. W., Dawson, J. M. UCLA Report No. PPG-802 (1984); *Bull. Am. Phys.* 29: 1355 (1984); Chen, P., Dawson, J. M., Huff, R. W., Katsouleas, T. *Phys. Rev. Lett.* 54: 693 (1985).

14. Palmer, R. B. *J. Appl. Phys.* 43: 3014 (1972).
15. Panofsky, W. K. H., Wenzel, W. A. *Rev. Sci. Inst.*, 27: 967 (1956).
16. See, for instance: Padamsee, H. *J. Superconductivity*, 1: 377 (1988).
17. Palmer, R. B. SLAC-PUB-4707 (1988); *Proc. DPF Summer Study Snowmass '88, Snowmass, CO, 1988*.
18. Wilson, P. B. SLAC-PUB-3985 (1986); *Proc. Stanford Linear Collider Conf., 1986*.
19. Chen, P., Yokoya, K. *Phys. Rev. D*38: 987 (1988); and "Disruption effects from the interaction of flat  $e^+ e^-$  beams," in preparation, to be submitted to *Phys. Rev. D*.
20. Chen, P. SLAC-PUB-4823 (1987); *Proc. Part. Acc. School, Batavia, IL, 1987*.
21. Minten, A. SLAC Internal Report CN-305.
22. Yokoya, K., Ruth, R. Pres. at *SLAC-KEK Collider Workshop, 1988*.
23. Sokolov, A. A., Ternov, I. M. *Synchrotron Radiation* (Berlin, Pergamon Press, 1968).
24. Himel, T., Siegrist, J. SLAC-PUB-3572; *Proc. Workshop on Laser Acc., Malibu, CA, AIP Conf. Proc.* 130: 602 (1985).
25. See, for instance, Blankenbeckler, R., Drell, S. D. *Phys. Rev. D*36: 277 (1987); Jakob, M., Wu, T. T. *Phys. Lett.* 197B: 253 (1987), and *Nucl. Phys.* B303: 373 and 389 (1988); Bell, M., Bell, J. S. *Part. Accel.* 22: 301 (1988).
26. Noble, R. SLAC-PUB-3871 (1986).
27. Zolotarev, M. S., Kuraev, E. A., Serbo, V. G. *Inst. Yadernoi Fiziki*, Preprint 81-63 (1981); SLAC TRANS-227 (1987).
28. Ginzburg, I. F., Kotkin, G. L., Serbo, V. G., Telnov, V.I. *Inst. Nucl. Phys., Novosibirsk* Preprint 81-102 (1981).

29. Chen, P. SLAC-PUB-4822 (1988); *Proc. DPF Summer Study Snowmass '88, Snowmass, CO, 1988.*
30. Chen, P., Telnov, V. I. SLAC-PUB-4923 (1989); *Phys. Rev. Lett.* 63: 1796.
31. See, for instance: Blankenbeckler, R., Drell, S. D., Kroll, N. SLAC-PUB-4954 (1989). Submitted to *Phys. Rev. D.*; Chen, P. SLAC-PUB-4823 (1989). *Proc. Part. Acc. School, Balavia, IL, 1987.*
32. Irwin, J. Private communication.
33. Palmer, R. B. SLAC-PUB-4295 (1987); *Proc. ICFA Workshop on New Dev. in Part. Acc. Techniques, Orsay, France, 1987*; CERN 87-11; ECFA 87-110.
34. Brown, K. Private communication.
35. Brown, K. L. SLAC-PUB-4159 (1986); *Proc. Topical Course on Frontiers on Part. Beams, South Padre Island, TX, 1986.*
36. Brown, K. Private communication.
37. Oide, K. SLAC-PUB-4806 (1988); *Proc. DPF Summer Study Snowmass '88, Snowmass, CO, 1988.*
38. Oide, K. *Phys. Rev. Lett.* 61: 1713 (1988).
39. Chen, P., Oide, K., Sessler, A. M., Yu, S. S. SLAC-PUB-5060 (1989); *Proc. XIV Int. Conf. on High Energy Acc., Tskuba, Japan, 1989.*
40. Spencer, J., Stucki, H. SLAC-PUB-4850 (1989); *Proc. Part. Acc. Conf., Chicago, IL, 1989.*
41. Egawa, K., Taylor, T. M. CERN CLIC Note 95, CERN LEP-MA/89-08; and the following reference.
42. Silverstroy, G. I., Skrinsky, A. N., Vsevolozhskaya, T. A. Superstrong quadrupoles of liquid metal for final focusing at linear colliders, preprint, INP, Novosibirsk, Russia.

43. Chen, P. *Part. Acc.* 20: 171 (1987); and has been discussed by many authors.
44. Chen, P., Su, J. J., Katsouleas, T., Wilks, S., Dawson, J. M. *IEEE Trans. Plasma Sci.* PS-15: 218 (1987); Cline, D. B., Cole, B., Rosenzweig, J. B., Norem, J. *Proc. 1987 Washington Acc. Conf.*, p. 241, Washington: IEEE.
45. Rosenzweig, J., et al., *Phys. Rev. Lett.* 61: 98 (1988).
46. Chen, P., Rajagopalan, S., Rosenzweig, J. *Phys. Rev.* D40: 926 (1989).
47. Palmer, R. B. SLAC-PUB-3688.
48. Farcas, Z. D., Wilson, P. B. SLAC-PUB-4088 (1985).
49. Wilson, P. B. SLAC-PUB-3674 (1985); *Proc. 2nd Workshop on Laser Acc., Malibu, CA, AIP Conf. Proc., 1985*, p. 130.
50. Bane, K. L. F. SLAC-PUB-3670 (1985); *Proc. Acc. Conf., Vancouver, B.C., Canada, 1985*.
51. Balakin, V., Novokhatski, A., Smirnov, V. *Proc. 12th Int. Conf. on High Energy Acc., FNAL, Batavia, IL, 1983*, p. 199.
52. Schnell, W. CLIC Note 34 (1987); Henke, H. CLIC Note 48 (1987).
53. Ruth, R. D. SLAC-PUB-4436 (1987), *Proc. US/CERN Joint Topical Course on Frontiers of Part. Beams, South Padre Island, TX, 1986*.
54. Fischer, G. E. SLAC-PUB-3392 (1985); *AIP Conf. Series Report No. 152, 1985*, p. 1260.
55. Palmer, R. B. SLAC Internal Reports AAS-23 (1986) & AAS-44 (1989); Palmer, R. B. SLAC-PUB-4433, submitted to *Part. Acc.*; Gluckstern, R. L. *Phys. Rev.* D39: 2780 (1989).
56. Palmer, R. B. SLAC-PUB-4542 (1988); *Proc. DPF Summer Study Snowmass '88, Snowmass, CO, 1988*; SLAC-Report-334.

57. Thompson, K. A., Ruth, R. D. SLAC-PUB-4801 (1989); *Phys. Rev. D*;  
Ruth, R. D. SLAC-PUB-4948 (1989); *Proc. 3rd Joint US-CERN School on  
Part. Acc., Capri, Italy, 1988.*
58. Kroll, N., Yu, S. Private communication.
59. Kroll, N., Farkas, D. Private communications.
60. Wang, J. W., Loew, G. A. SLAC-PUB-4866 (1989); *Proc. IEEE Part. Acc.  
Conf., Chicago, IL, 1989.*
61. Juetner, B., et al. *Beitrage für plasmaphysik* 10: 383 (1970).
62. Kroll, N. M. *AIP Conf. Proc.* 130, p. 296 (1985).
63. Wilson, I. CERN CLIC Note 52 (1987).
64. Eppley, K. SLAC-PUB-4900 (1989); *Proc. IEEE Part. Acc. Conf., Chicago,  
IL, 1989.* The tube has recently operated at over 60 MW; Lee, T. Private  
communication.
65. Toshiba Corp. Presented at *Int. Conf. on High Energy Acc., Tsukuba, Japan,  
1989.*
66. Sinclair, C. K. SLAC-PUB-4111 (1986); Fukushima, Y., et al. *Nucl. Instrum.  
Methods A238*: 215 (1985).
67. Budker, G. I., et al. *Part. Acc.*, 10: 41 (1979).
68. Orzechawski, et al. *Phys. Rev. Lett.* 58: 2172 (1986).
69. Hopkins, D. B., et al. *Proc. 1988 Linear Acc. Conf., Williamsburg, VA, 1988.*
70. Allen, M. A., et al. *Proc. European Part. Acc. Conf., Rome, Italy, 1988*; Yu, S.,  
et al. Pres. at *Baltimore APS Conf., 1989.*
71. Granetstein, V. L., et al. *Proc. SPIE Tech. Symp. Southeast, Orlando, FL,  
1987.*

72. Eppley, K., Miller, R., Herrmannsfeldt, W. *Trans IEEE Part. Acc. Conf., Washington, D.C., 1987.*
73. Palmer, R. *Proc. Workshop on New Dev. in Part. Acc. Techniques, Orsay, France, 1987*, p. 272.
74. Bizek, H. M., McIntyre, P. M., Raparia, D., Swenson, C. A. *Proc. Workshop on New Dev. in Part. Acc. Techniques, Orsay, France, 1987*, p. 264.
75. Boyd, M. R., Dehn, R. A., Hickey, J. S., Mihran, T. G. *IRE Trans. on Electron Devices*, p. 247 (1962).
76. Palmer, R. B., Herrmannsfeldt, W. B., Eppley, K. R. SLAC-PUB-5026; *Proc. Int. Conf. on High Energy Acc., Tsukuba, Japan, 1989.*
77. McDowell, H. L., Feinstein, J. *Proc. 4th Int. Congr. Microwave Tubes, Scheveningen, 1962*, p. 179.
78. Farcas, Z. D. SLAC-PUB-3694 (1986); *IEEE Trans. Microwave Theory and Techniques*, MTT-34: 1036 (1986).
79. Wilson, P. B., Farkas, Z. D., Ruth, R. D. SLAC AP-78 (1990).
80. Sinclair, C. K., et al. *Proc. Argonne Conf. on High Energy Physics with Polarized Beams and Targets, 1976.*
81. Fischer, J., Srinivasan-Rao, T. *Proc. ICFA Workshop on New Dev. in Part. Acc. Techniques, Orsay, France, 1987*, p. 506.
82. Kheifets, S. A., Ruth, R. D., Fieguth, T. H. SLAC-PUB-5034 (1989); *Proc. Int. Conf. on High Energy Acc., Tsukuba, Japan, 1989.*
83. Steffen, K. Internal Report DEST-PET-79/05 (1979); Palmer, R. B. SLAC-PUB-3883 (1985), *Proc. Sem. on New Tech. for Future Acc., Erice, Italy, 1986.*

84. Sands, M. SLAC-PUB-121, p. 110 (1979).
85. Bisognano, J., et al. LBL-19771 (1985).
86. Raubenheimer, T. O., et al. SLAC-PUB-4918 (1989); *Proc. IEEE Part. Acc. Conf., Chicago, IL, 1989.*
87. Krejcik, P. CERN CLIC Note 67 (1988).
88. Blankenbeckler, R. Drell, S. D. *Proc. DPF Summer Study Snowmass '88, Snowmass, CO, 1988*; SLAC-PUB-4810.

**Table 1** Parameters of single bunch 0.5 TeV colliders based on different philosophies

|                          |                             | A    | B    | C    | D    | E    |
|--------------------------|-----------------------------|------|------|------|------|------|
|                          |                             | 0°   | 0°   | Flat | Crab | Crab |
|                          |                             |      | 5T   |      |      | 1 cm |
| <i>General</i>           |                             |      |      |      |      |      |
| c-of-mass $E$            | TeV $E$                     | 0.50 | 0.50 | 0.50 | 0.50 | 0.50 |
| luminosity               | $10^{33}$ cgs $\mathcal{L}$ | 0.24 | 0.56 | 0.34 | 1.2  | 1.8  |
| wall power               | MW $W$                      | 70.0 | 70.0 | 70.0 | 70.0 | 70.0 |
| length overall           | km $\ell$                   | 6.87 | 6.87 | 7.07 | 6.87 | 6.87 |
| spot height              | nm $\sigma_y$               | 44.7 | 29.3 | 7.0  | 15.7 | 8.5  |
| aspect ratio             | $R$                         | 25.5 | 25.5 | 180  | 38.7 | 15.5 |
| init. inv emit           | mm mrad $\epsilon_x$        | 13.4 | 13.4 | 9.67 | 13.4 | 1.91 |
| emittance $x/y$          | $R_\epsilon$                | 100  | 100  | 100  | 100  | 37   |
| rep. rate                | Hz $f$                      | 115  | 115  | 110  | 115  | 794  |
| $N/\text{bunch}$ (init)  | $10^{10}$ $N$               | 11.6 | 11.6 | 7.7  | 11.6 | 1.7  |
| loading                  | % $\eta$                    | 12   | 12   | 8    | 12   | 12   |
| rf source eff            | % $\eta_{rf}$               | 20.0 | 20.0 | 20.0 | 20.0 | 20.0 |
| <i>Intersection</i>      |                             |      |      |      |      |      |
| bunch length             | mm $\sigma_z$               | 0.32 | 0.32 | 0.11 | 0.32 | 0.12 |
| disruption               | $D_y$                       | 5.5  | 12.8 | 7.3  | 29.7 | 13.5 |
| disrpt. enhance          | $H$                         | 2.33 | 2.29 | 1.68 | 2.22 | 2.60 |
| crossing angle           | mrad $\theta_c$             | 0    | 0    | 10   | 50   | 50   |
| $\sigma_y/\sigma$ (Oide) | Oide fac                    | 9.6  | 6.3  | 1.9  | 3.4  | 3.6  |
| $\sigma_z/\beta_y^*$     | $A$                         | 0.07 | 0.17 | 0.71 | 0.59 | 0.29 |
| quantum $E/E_{crit}$     | $\gamma$                    | 0.10 | 0.15 | 0.19 | 0.20 | 0.40 |
| beamstrahlung            | $dE/E$ $\delta$             | 0.09 | 0.18 | 0.08 | 0.29 | 0.29 |

Table 1 Continued

|                    |                       | A    | B    | C    | D    | E    |
|--------------------|-----------------------|------|------|------|------|------|
|                    |                       | 0°   | 0°   | Flat | Crab | Crab |
|                    |                       |      | 5T   |      |      | 1 cm |
| <i>Final focus</i> |                       |      |      |      |      |      |
| vert focus         | mm $\beta_y^*$        | 4.35 | 1.86 | 0.15 | 0.54 | 0.41 |
|                    | $\beta_x^*/\beta_y^*$ | 6.5  | 6.5  | 324  | 15.0 | 6.5  |
| $dp/p$ for focus   | % $\delta_f$          | 0.22 | 0.22 | 0.20 | 0.22 | 0.24 |
| final quad aps     | mm $R_q$              | 292  | 191  | 0.5  | 4.5  | 1.9  |
| free length        | m $\beta_1$           | 14.5 | 6.20 | 0.63 | 1.80 | 1.18 |
| pole field         | T $B_q$               | 1.40 | 5.00 | 1.40 | 1.40 | 1.40 |
| <i>Wakes</i>       |                       |      |      |      |      |      |
| uncorr. emit gain  | $C_W$                 | 14.9 | 14.9 | 4.4  | 14.9 | 23.5 |
| $dp/p$ BNS         | % $\delta_{BNS}$      | 3.33 | 3.33 | 0.82 | 3.33 | 3.33 |
| $\Delta$ phase adv | $\Delta\Phi$          | 10.5 | 10.5 | 2.8  | 10.5 | 17.0 |
| toll from $dp/p$   | $\mu\text{m } dx_d$   | 1.8  | 1.8  | 1.5  | 1.8  | 0.9  |
| vib tol            | nm $dx_v$             | 62.8 | 41.7 | 55.9 | 8.4  | 14.7 |
| phase for BNS      | deg. $\Phi_{BNS}$     | 5.0  | 5.0  | 27.3 | 5.0  | 5.0  |
| <i>Rf</i>          |                       |      |      |      |      |      |
| wavelength         | mm $\lambda$          | 26.2 | 26.2 | 26.2 | 26.2 | 10.0 |
| max accel grad     | MeV/m $G$             | 100  | 100  | 100  | 100  | 100  |
| iris rad/lambda    | $a/\lambda$           | 0.20 | 0.20 | 0.20 | 0.20 | 0.20 |
| rf pulse length    | ns $t$                | 82.1 | 82.1 | 82.1 | 82.1 | 19.3 |
| peak power/m       | GW/m P/m              | 0.24 | 0.24 | 0.24 | 0.24 | 0.15 |
| total rf energy    | kJ $J$                | 121  | 121  | 128  | 121  | 17.6 |
| <i>Damping</i>     |                       |      |      |      |      |      |
| wiggler field      | T $B_D$               | 2.0  | 2.0  | 2.0  | 2.0  | 2.0  |
| partition fun $x$  | $J_x$                 | 1.0  | 1.0  | 1.0  | 1.0  | 1.0  |
| $E$ of ring        | GeV $E$               | 0.86 | 0.86 | 0.89 | 0.86 | 0.86 |
| bunch len          | $\sigma_z$            | 3.7  | 3.7  | 3.5  | 3.7  | 3.7  |
| cooling time       | msec $t$              | 2.68 | 2.68 | 2.58 | 2.68 | 2.69 |
| tune $x$           | $Q_x$                 | 8.6  | 8.6  | 10.6 | 8.6  | 22.5 |

Table 2 Parameters of multibunch 0.5 TeV colliders based on different philosophies

|                          |                             | F<br>Flat | G<br>Crab | H<br>Crab<br>1 cm |
|--------------------------|-----------------------------|-----------|-----------|-------------------|
| <i>General</i>           |                             |           |           |                   |
| c-of-mass $E$            | TeV $E$                     | 0.50      | 0.50      | 0.50              |
| luminosity               | $10^{33}$ cgs $\mathcal{L}$ | 1.37      | 5.85      | 4.12              |
| wall power               | MW $W$                      | 70.0      | 70.0      | 70.0              |
| length overall           | km $\ell$                   | 6.58      | 6.58      | 6.29              |
| spot height              | nm $\sigma_y$               | 3.4       | 6.5       | 5.6               |
| aspect ratio             | $R$                         | 180       | 25.5      | 3.6               |
| init. inv emit           | mm mrad $\epsilon_x$        | 3.77      | 3.77      | 0.19              |
| emittance $x/y$          | $R_c$                       | 100       | 100       | 2                 |
| rep. rate                | Hz $f$                      | 130       | 130       | 913               |
| $N/\text{bunch}$ (init)  | $10^{10}$ $N$               | 2.41      | 2.41      | 0.18              |
| loading                  | % $\eta$                    | 2.50      | 2.50      | 1.25              |
| no. of bunches           | $Nb$                        | 10        | 10        | 20                |
| total loading            | % $\eta_t$                  | 25        | 25        | 25                |
| rf source eff            | % $\eta_{rf}$               | 20        | 20        | 20                |
| <i>Intersection</i>      |                             |           |           |                   |
| bunch length             | mm $\sigma_z$               | 0.11      | 0.11      | 0.04              |
| disruption               | $D_y$                       | 9.6       | 17.8      | 3.9               |
| disrpt. enhance          | $H$                         | 1.56      | 2.25      | 2.23              |
| crossing angle           | mrad $\theta_c$             | 5.7       | 50        | 50                |
| $\sigma_y/\sigma$ (Oide) | Oide fac                    | 1.8       | 3.5       | 1.6               |
| $\sigma_z/\beta_y^*$     | $A$                         | 1.17      | 0.31      | 0.41              |
| bunch separation         | m $\Delta z$                | 0.29      | 0.29      | 0.03              |
| multibunch instab        | $C_n$                       | 1.4       | 1.0       | 1.0               |
| quantum $E/E_{crit}$     | $\gamma$                    | 0.12      | 0.45      | 0.75              |
| beamstrahlung            | $dE/E$ $\delta$             | 0.04      | 0.30      | 0.23              |

Table 2 Continued

|                       |                     | F<br>Flat | G<br>Crab | H<br>Crab<br>1 cm |
|-----------------------|---------------------|-----------|-----------|-------------------|
| <i>Final focus</i>    |                     |           |           |                   |
| vert focus            | mm $\beta_y^*$      | 0.09      | 0.33      | 0.10              |
| $\beta_x^*/\beta_y^*$ | $R$                 | 324       | 6.5       | 6.5               |
| $dp/p$ for focus      | % $\delta_f$        | 0.17      | 0.17      | 0.12              |
| final quad aps        | mm $R_q$            | 0.4       | 4.7       | 0.8               |
| free length           | m $\ell_1$          | 0.50      | 1.85      | 0.76              |
| pole field            | T $B_q$             | 1.4       | 1.4       | 1.4               |
| <i>Wakes</i>          |                     |           |           |                   |
| uncorr. emit gain     | $C_W$               | 2.1       | 2.1       | 2.4               |
| $dp/p$ BNS            | % $\delta_{BNS}$    | 0.26      | 0.26      | 0.32              |
| $\Delta$ phase adv    | $\Delta\Phi$        | 1.41      | 1.41      | 1.46              |
| toll from $dp/p$      | $\mu\text{m } dx_d$ | 33.6      | 33.6      | 52.1              |
| vib tol               | nm $dx_v$           | 23.0      | 12.5      | 46.6              |
| phase for BNS         | deg. $\Phi_{BNS}$   | 14.3      | 14.3      | 3.1               |
| <i>Rf</i>             |                     |           |           |                   |
| wavelength            | mm $\lambda$        | 26.2      | 26.2      | 10.0              |
| max accel grad        | MeV/m $G$           | 100       | 100       | 100               |
| iris rad/lambda       | $a/\lambda$         | 0.20      | 0.20      | 0.20              |
| rf pulse length       | ns $t$              | 82.1      | 82.1      | 19.3              |
| peak power/m          | GW/m $P/m$          | 0.24      | 0.24      | 0.15              |
| total rf energy       | kJ $J$              | 107       | 107       | 15.3              |
| <i>Damping</i>        |                     |           |           |                   |
| wiggler field         | T $B_D$             | 2.0       | 2.0       | 2.0               |
| partition fun $x$     | $J_x$               | 1.0       | 1.0       | 1.0               |
| $E$ of ring           | GeV $E$             | 1.00      | 1.00      | 0.59              |
| bunch len             | $\sigma_z$          | 3.0       | 3.0       | 2.3               |
| bunch len/sep         | $\sigma_z/\Delta z$ | 0.10      | 0.10      | 0.66              |
| cooling time          | msec $t$            | 2.31      | 2.31      | 3.88              |
| tune $x$              | $Q_x$               | 19.5      | 19.5      | 37.7              |

**Table 3** Parameters of multibunch crab-crossing colliders, at different center-of-mass energies

|                          |                             | I    | J    | K    | L     | M     |
|--------------------------|-----------------------------|------|------|------|-------|-------|
|                          |                             | ILC  | TLC  | 5TLC | 10TLC | SLC   |
| <i>General</i>           |                             |      |      |      |       |       |
| c-of-mass $E$            | TeV $E$                     | 0.50 | 1.00 | 5.00 | 10.00 | 0.10  |
| luminosity               | $10^{33}$ cgs $\mathcal{L}$ | 2.54 | 11.1 | 278  | 1130  | 0.002 |
| wall power               | MW $W$                      | 70   | 100  | 200  | 300   | 26    |
| length overall           | km $\ell$                   | 6.6  | 8.5  | 27.3 | 36.2  | 3.0   |
| spot height              | nm $\sigma_y$               | 4.0  | 3.1  | 0.2  | 0.1   | 1463  |
| aspect ratio             | $R$                         | 109  | 62   | 136  | 265   | 1     |
| init. inv emit           | mm mrad $c_x$               | 3.77 | 3.41 | 0.29 | 0.16  | 30.0  |
| emittance $x/y$          | $R_c$                       | 100  | 100  | 200  | 300   | 1     |
| ref. rate                | Hz $f$                      | 130  | 128  | 169  | 148   | 120   |
| $N/\text{bunch}$ (init)  | $10^{10}$ $N$               | 2.41 | 2.13 | 0.31 | 0.40  | 5.00  |
| loading                  | % $\eta$                    | 2.50 | 1.47 | 0.60 | 0.60  | 3.23  |
| no. of bunches           | $Nb$                        | 10   | 17   | 125  | 125   | 1     |
| total loading            | % $\eta_t$                  | 25   | 25   | 75   | 75    | 3.23  |
| rf source eff            | % $\eta_{rf}$               | 20   | 40   | 40   | 60    | 12    |
| <i>Intersection</i>      |                             |      |      |      |       |       |
| bunch length             | mm $\sigma_z$               | 0.11 | 0.12 | 0.02 | 0.015 | 1.05  |
| disruption               | $D_y$                       | 11.4 | 16.9 | 7.3  | 11.0  | 0.7   |
| disrpt. enhance          | $H$                         | 1.74 | 1.89 | 2.07 | 2.21  | 1.94  |
| crossing angle           | mrad $\theta_c$             | 50   | 50   | 100  | 100   | 0     |
| $\sigma_y/\sigma$ (Oide) | Oide fac                    | 2.1  | 1.8  | 1.1  | 1.0   | 9.6   |
| $\sigma_z/\beta_y^*$     | $A$                         | 0.84 | 0.73 | 0.21 | 0.19  | 0.15  |
| bunch separation         | m $\Delta z$                | 0.29 | 0.17 | 0.03 | 0.02  | 0.00  |
| quantum $E/E_{crit}$     | $\gamma$                    | 0.17 | 0.60 | 21   | 70    | 0.002 |
| beamstrahlung            | $dE/E$ $\delta$             | 0.07 | 0.26 | 0.27 | 0.30  | 0.001 |

Table 3 Continued

|                       |                     | I    | J    | K    | L     | M    |
|-----------------------|---------------------|------|------|------|-------|------|
|                       |                     | ILC  | TLC  | 5TLC | 10TLC | SLC  |
| <i>Final focus</i>    |                     |      |      |      |       |      |
| vert focus            | mm $\beta_y^*$      | 0.13 | 0.16 | 0.08 | 0.08  | 7.00 |
| $\beta_x^*/\beta_y^*$ | $R$                 | 120  | 38   | 96   | 265   | 1    |
| $dp/p$ for focus      | % $\delta_f$        | 0.17 | 0.09 | 0.07 | 0.07  | 0.45 |
| final quad aps        | mm $R_q$            | 0.7  | 1.5  | 0.10 | 0.03  | 49.1 |
| free length           | m $\ell_1$          | 0.70 | 1.47 | 0.86 | 0.81  | 3.16 |
| pole field            | T $B_q$             | 1.4  | 1.4  | 1.4  | 0.94  | 1.4  |
| <i>Wakes</i>          |                     |      |      |      |       |      |
| uncorr. emit gain     | $C_W$               | 2.1  | 2.0  | 1.3  | 1.3   | 6.8  |
| $dp/p$ BNS            | % $\delta_{BNS}$    | 0.26 | 0.25 | 0.03 | 0.04  | 2.26 |
| $\Delta$ phase adv    | $\Delta\Phi$        | 1.41 | 0.91 | 1.44 | 1.33  | 4.46 |
| toll from $dp/p$      | $\mu\text{m } dx_d$ | 34   | 41   | 5    | 2.7   | 77.0 |
| vib tol               | nm $dx_v$           | 27.1 | 11.5 | 2.64 | 1.1   | 2052 |
| phase for BNS         | deg. $\Phi_{BNS}$   | 14.3 | 5.5  | 11.2 | 8.5   | -3.9 |
| <i>Rf</i>             |                     |      |      |      |       |      |
| wavelength            | mm $\lambda$        | 26.2 | 26.2 | 12.0 | 10.0  | 105  |
| max accel grad        | MeV/m $G$           | 100  | 150  | 200  | 300   | 20   |
| iris rad/lambda       | $a/\lambda$         | 0.20 | 0.20 | 0.25 | 0.30  | 0.11 |
| rf pulse length       | ns $t$              | 82.1 | 82.1 | 16.4 | 12.1  | 919  |
| peak power/m          | GW/m P/m            | 0.24 | 0.54 | 1.12 | 2.93  | 0.10 |
| total rf energy       | kJ $J$              | 107  | 312  | 474  | 1218  | 26   |
| <i>Damping</i>        |                     |      |      |      |       |      |
| wiggler field         | T $B_D$             | 2    | 2    | 2    | 4     | 2    |
| partition fun $x$     | $J_x$               | 1    | 1    | 2.5  | 2.5   | 1    |
| $E$ of ring           | GeV $E$             | 1.00 | 1.01 | 2.45 | 1.77  | 1.20 |
| bunch len             | cm $\sigma_z$       | 3.0  | 2.9  | 0.2  | 0.4   | 1.1  |
| bunch len/sep         | $\sigma_z/\Delta z$ | 0.10 | 0.17 | 0.08 | 0.21  | —    |
| cooling time          | msec $t$            | 2.31 | 2.28 | 0.94 | 0.32  | 2.45 |
| tune $x$              | $Q_x$               | 19.5 | 20.9 | 137  | 175   | 5.7  |

### Figure Captions

- 1) Types of collider: (a) circular proton-proton, (b) circular electron-positron, (c) SLC, and (d) linear electron-positron.
- 2) The center of mass "available" energy of various colliders, plotted against the circumference or total length of each machine. The available energy for proton or antiproton machines is taken to be one-tenth of the total energy. (a) for circular electron-positron machines; (b) for circular proton or antiproton machines; and (c) for linear electron-positron machines.
- 3) Accelerating gradient limits from different causes: (a) electrical breakdown, (b) surface melting of the structure, and (c) fatigue damage of the structure. The continuous lines are for rf structures with a pulse length equal to the filling (or loss) time. The dashed lines are for single pulse structures.
- 4) Lines of constant costs on an accelerating gradient vs. wavelength plot. The dashed line represents that gradient for minimum cost at a given wavelength.
- 5) Luminosity of some representative electron-positron colliders plotted versus their center-of-mass energies. The line represent colliders yielding 10,000 events per unit of  $R$ , per year (defined as  $10^7$  sec): a reasonable requirement for future linear colliders.
- 6) Crab crossing.
- 7) Luminosity enhancement factors for round beams, as a function of the disruption parameter  $D$  and  $A$ , the ratio of bunch length  $\sigma_z$  to the focus strength  $\beta^*$ .
- 8) Luminosity enhancement factors for flat beams, as a function of the disruption parameter  $D_y$  and  $A_y$ , the ratio of bunch length  $\sigma_z$  to the focus strength  $\beta_y^*$ .
- 9) Enhancement of alignment sensitivity  $C_D$  as a function of the disruption parameter  $D_y$ , for flat beams.

- 10) The beamstrahlung factor  $H_Y$  as a function of  $Y$  as shown by Noble (dotted line) and from Eq. 26 (dots). The product  $YH_Y$  is also shown (line); the beamstrahlung energy loss  $\delta$  is proportional to this product.
- 11) Auxiliary functions  $\Xi$  and  $\Omega$  of the real and virtual coherent-pair-creation probabilities.
- 12) Possible small bore quadrupole magnet designs: (a) long pole tip, conductor driven; (b) all permanent magnet; and (c) long pole, permanent magnet driven.
- 13) Parameters of a SLAC-like accelerating cavity as a function of the group velocity  $v_g/c = \beta_g$ : (a) the iris radius  $a$  divided by wavelength  $\lambda$ ; (b) the normalized corrected elastance  $s_{at}$ ; (c) the attenuation time constant  $t_0$  in  $\mu\text{sec}$ , for  $\lambda = 10.5$  cm; (d) the peak rf field in the cavity  $\mathcal{E}_{pk}$  divided by the average accelerating field  $\mathcal{E}_a$ ; (e) the outer cavity radius  $b$  divided by the iris radius  $a$ ; and (f) the relative peak rf power.
- 14) The scale invariant transverse wakefield ( $a^3 W_t$ ) as a function of the distance  $z$  divided by the iris radius  $a$  for (dashed)  $a/\lambda = 0.105$  (as for SLC), and (line)  $a/\lambda = 0.2$ .
- 15) The scale invariant longitudinal wakefield ( $a^2 W_l$ ) as a function of the length  $z$  divided by the iris radius  $a$ , for  $a/\lambda = 0.2$ .
- 16) The longitudinal wakefield-generated momentum spread, for a Gaussian bunch passing through a SLAC-like structure.
- 17) Accelerating structure with slotted irises and waveguides to damp transverse modes.
- 18) Concepts of rf power supplies: (a) klystron, (b) lasertron, (c) relativistic klystron, (d) two-beam accelerator, (e) cluster klystron, and (f) cross-field amplifier.

- 19) Klystron efficiencies plotted as a function of perveance. The wavelengths of each example are given in parentheses. The line represents an approximate fit to the data.
- 20) Rf pulse compression: (a) SLED, (b) binary pulse compression, and (c) super-SLED.
- 21) The normalized emittance of a sample damping ring, as a function of operating electron energy. As  $E$  is varied the ring is varied to keep the bending field  $B_d$ , the focusing field  $B_f$  and the tune  $Q$  fixed. At low energies, the emittance is dominated by intrabeam scattering; at high energies, by quantum fluctuations.
- 22) A simplified diagram of the interdependence of collider parameters.
- 23) Luminosity for different aspect ratios, plotted against the beamstrahlung parameter  $\delta$ , for a 0.5 TeV, crab crossing, multibunch collider.

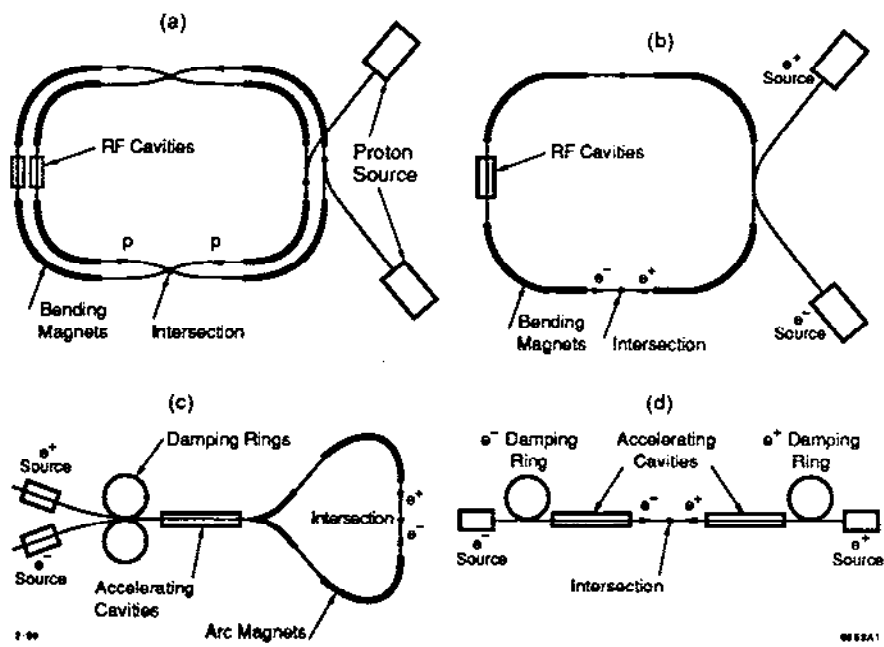


Fig. 1

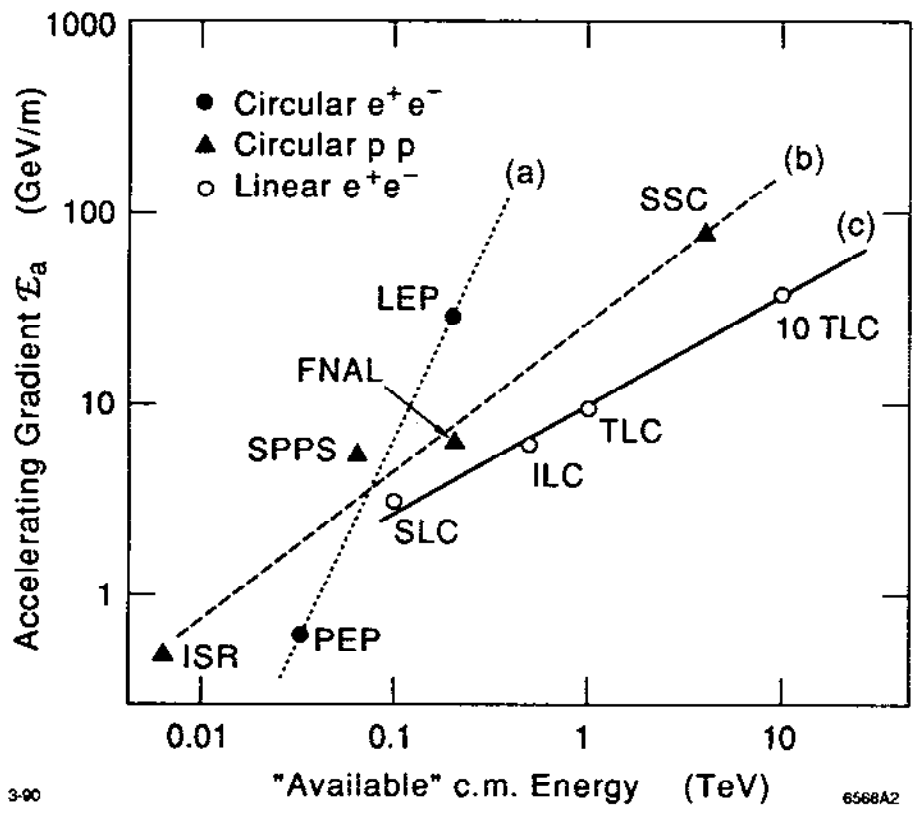


Fig. 2

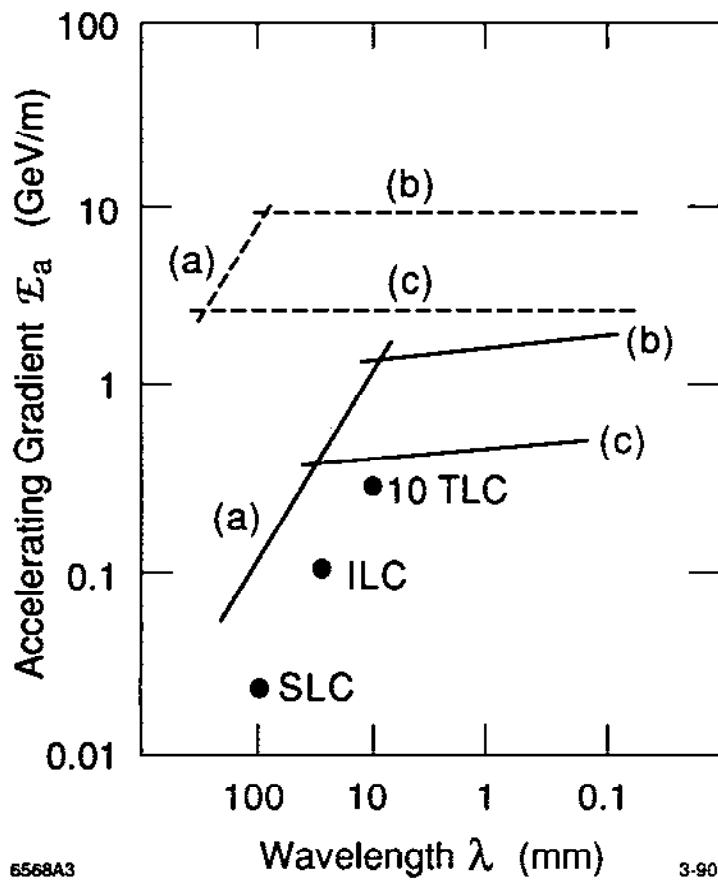


Fig. 3

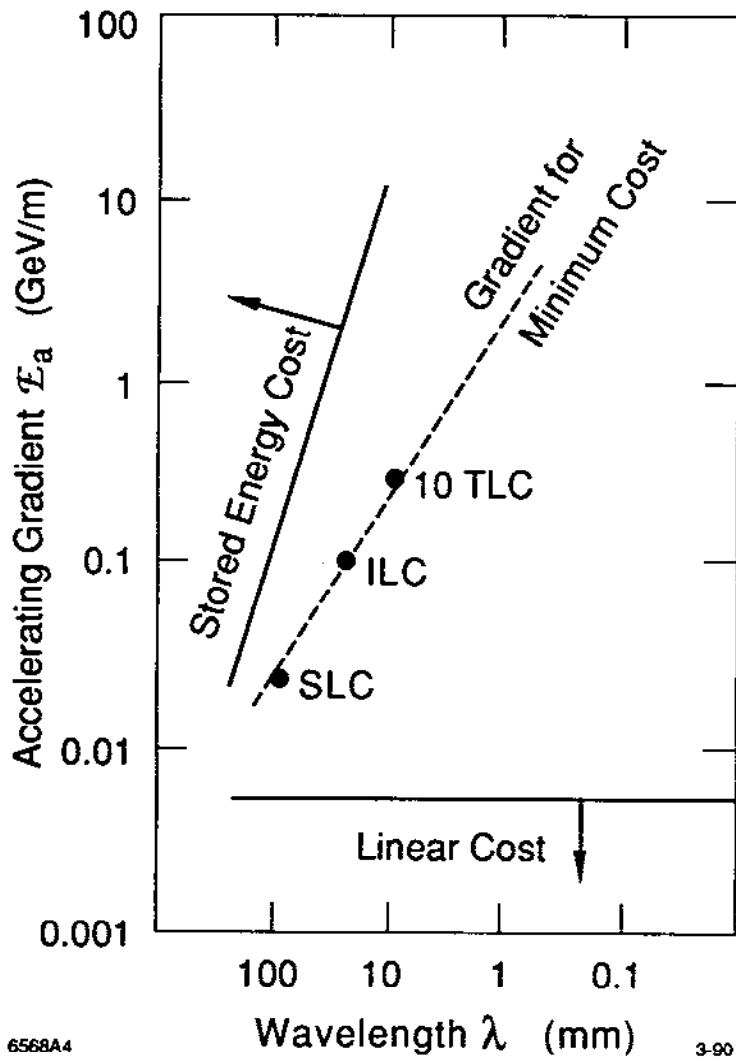


Fig. 4

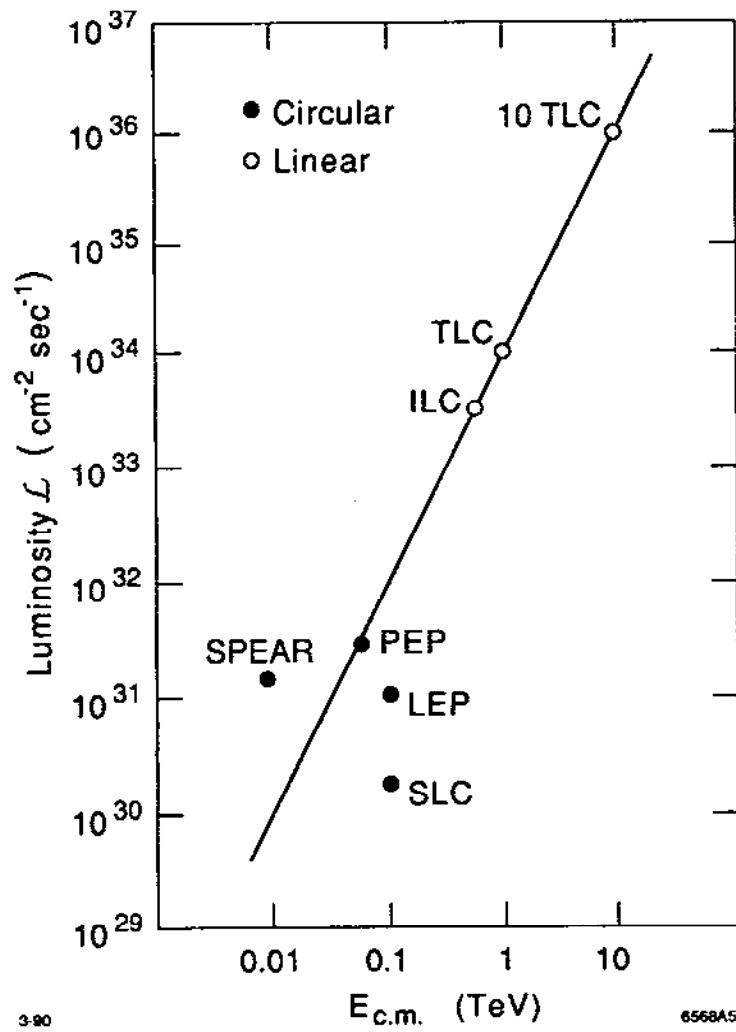


Fig. 5

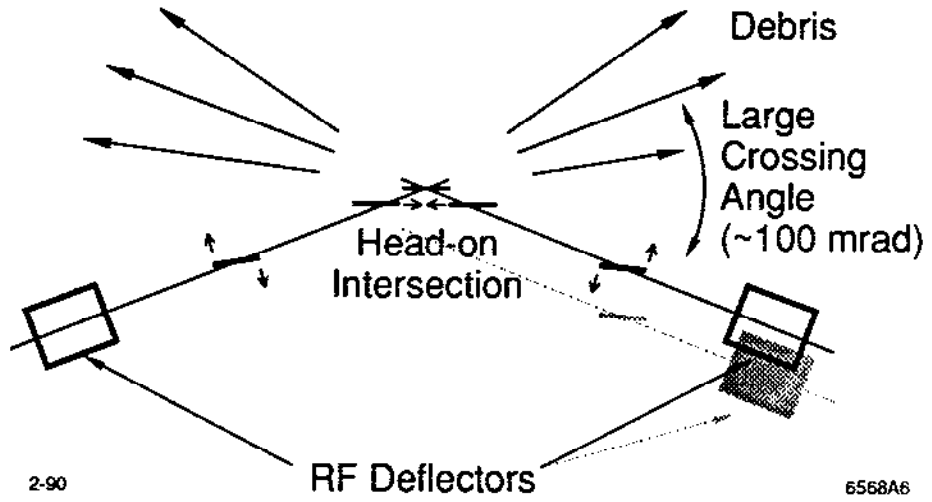
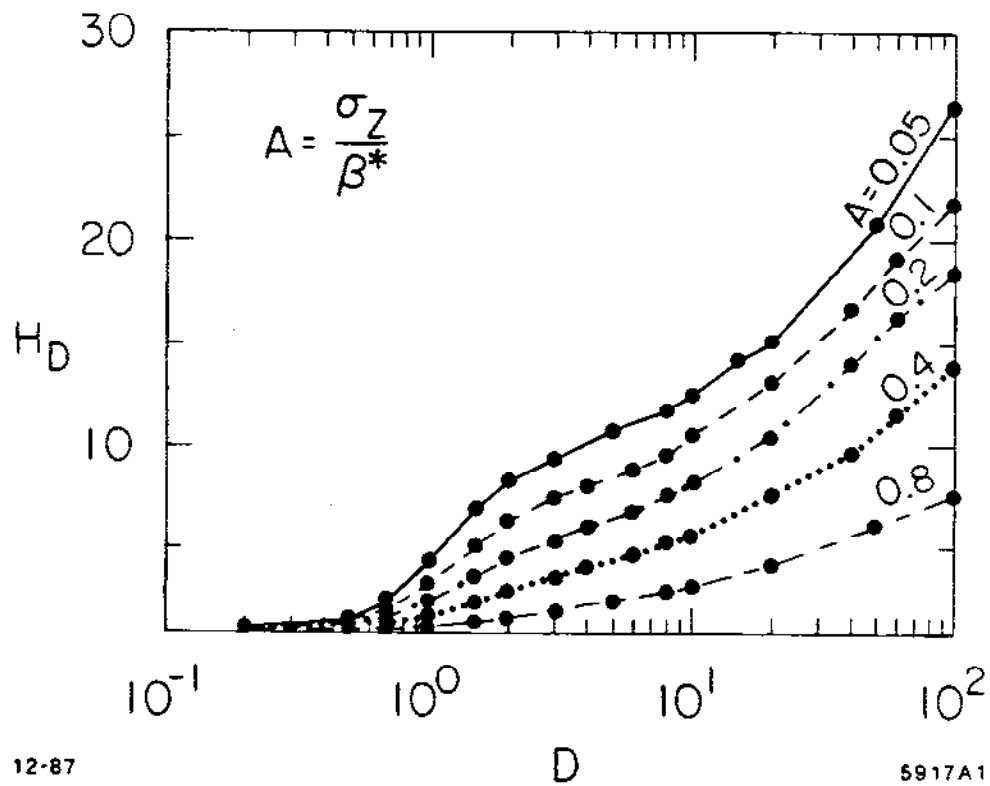


Fig. 6



12-87

Fig. 7

5917A1

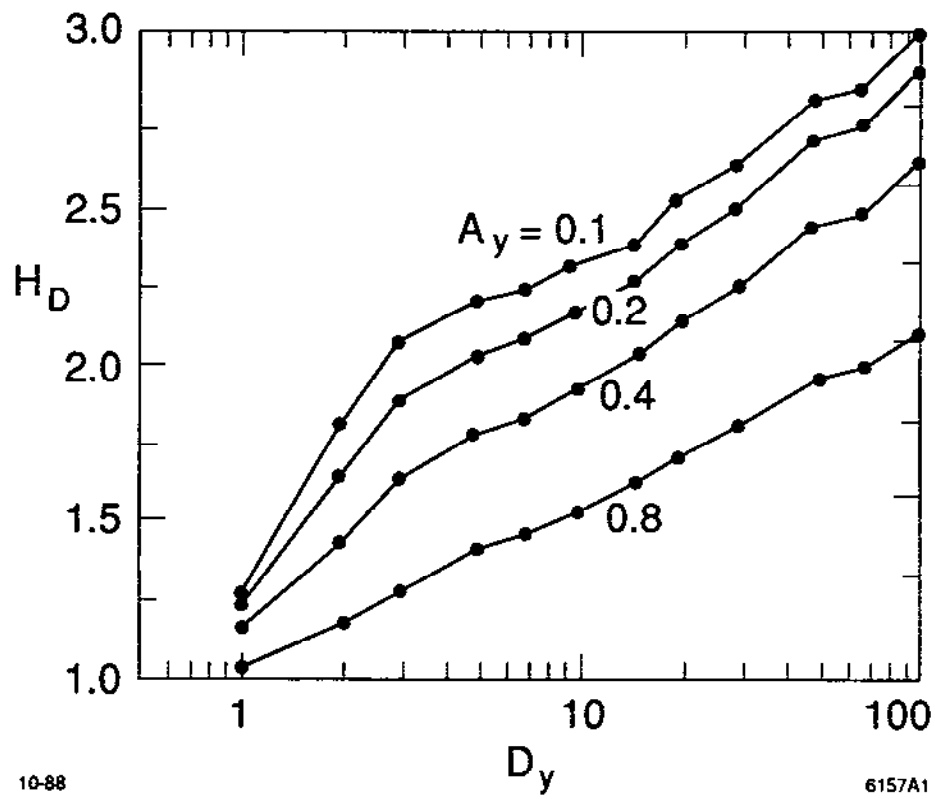
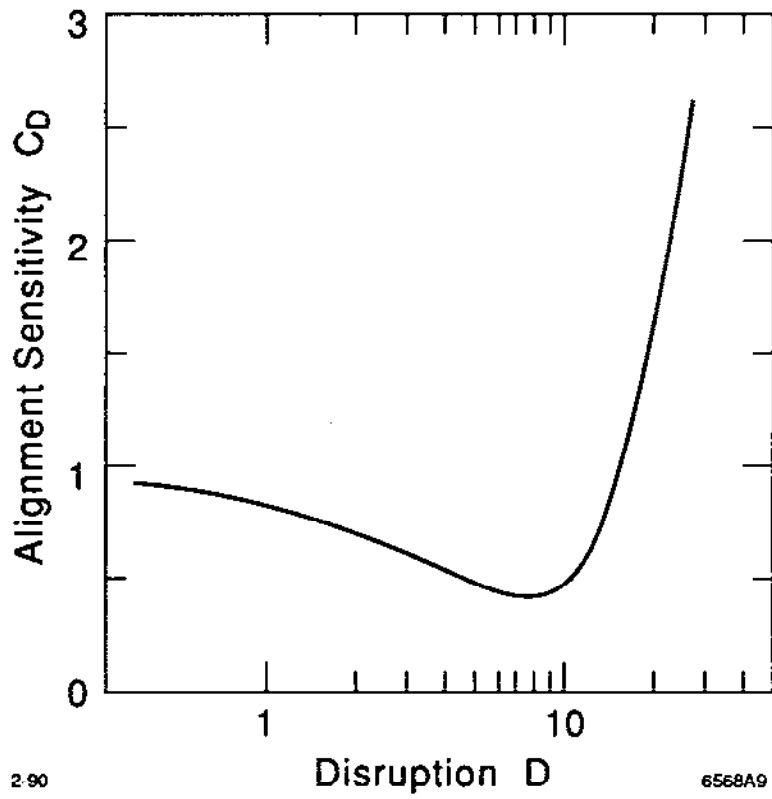


Fig. 8



2.90

6568A9

Fig. 9

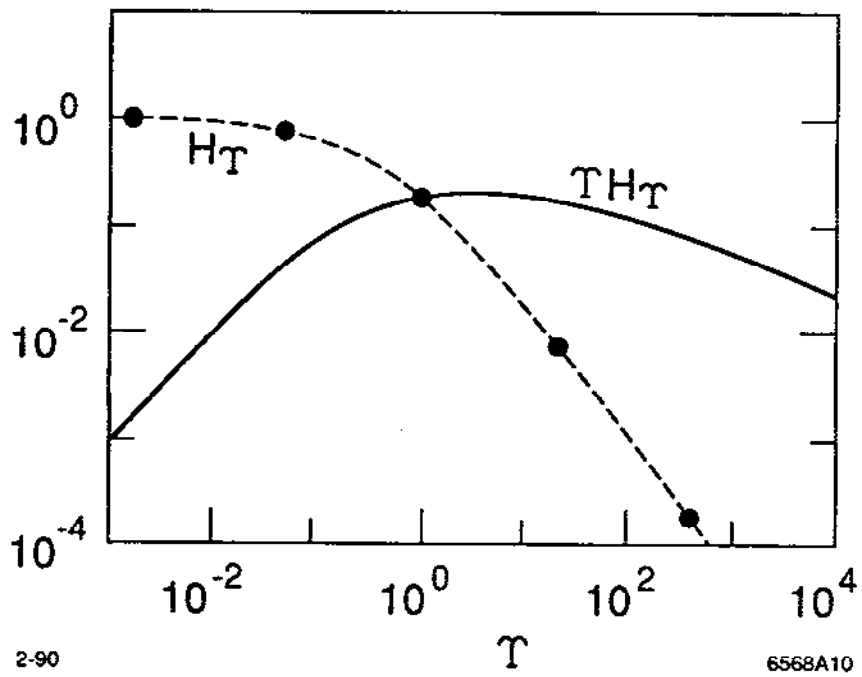


Fig. 10

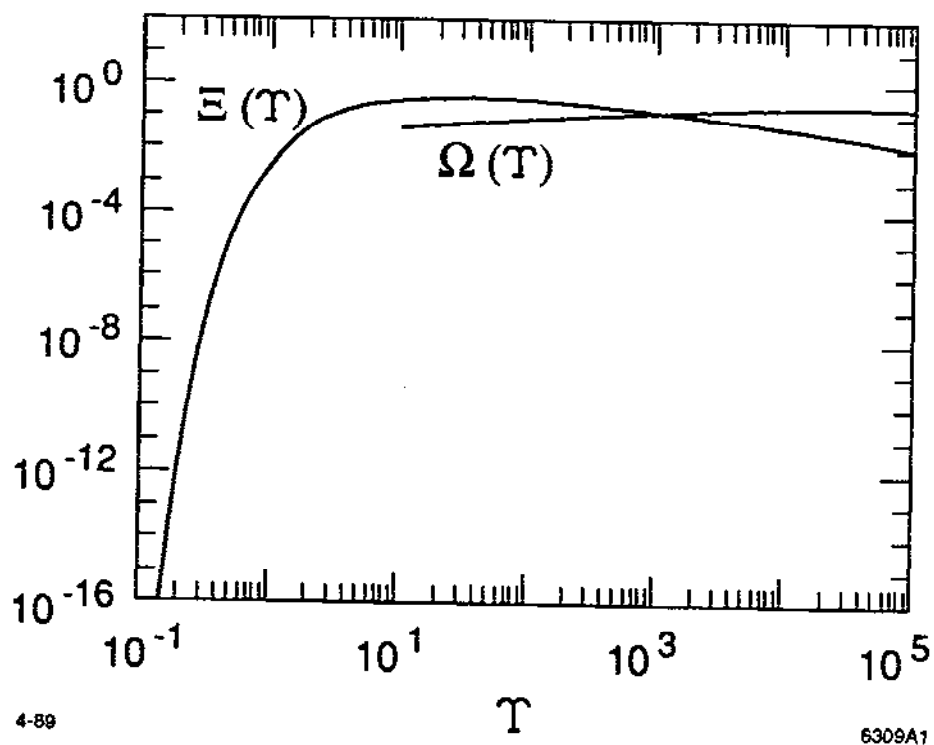


Fig. 11

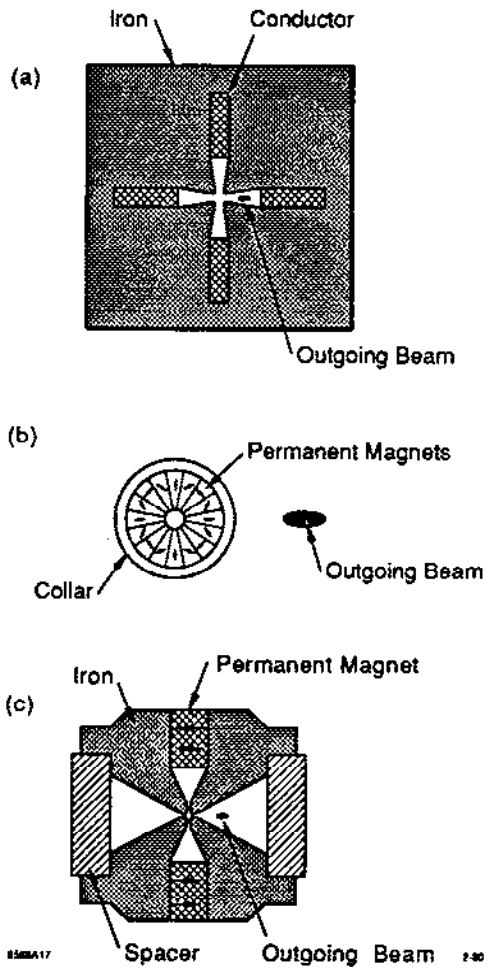


Fig. 12

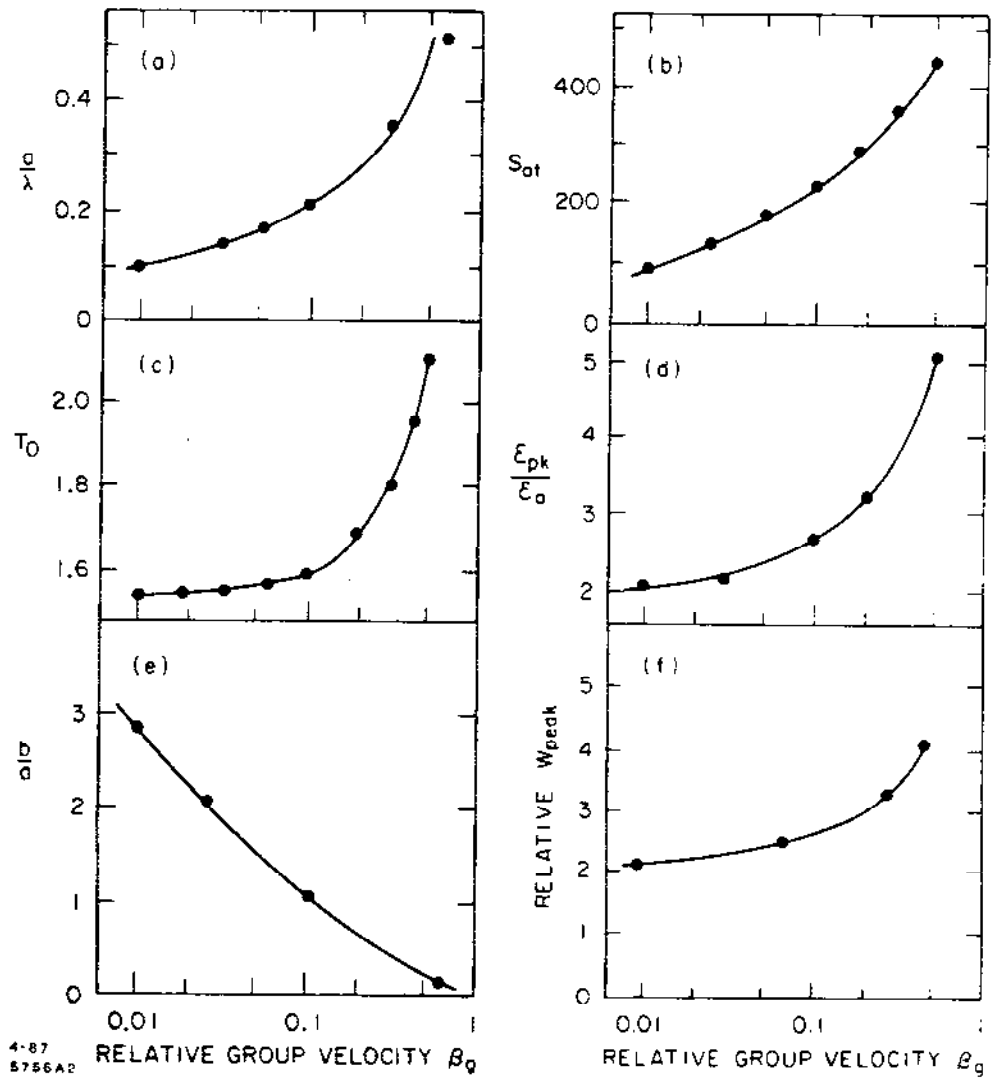


Fig. 13

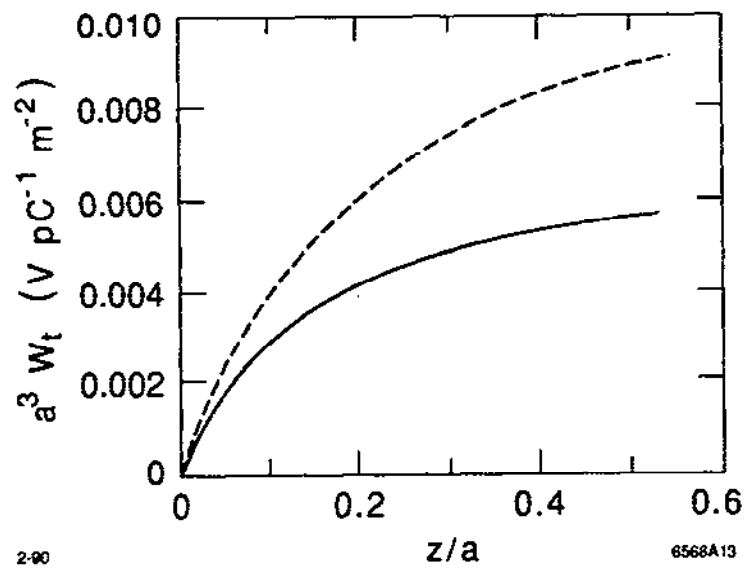


Fig. 14

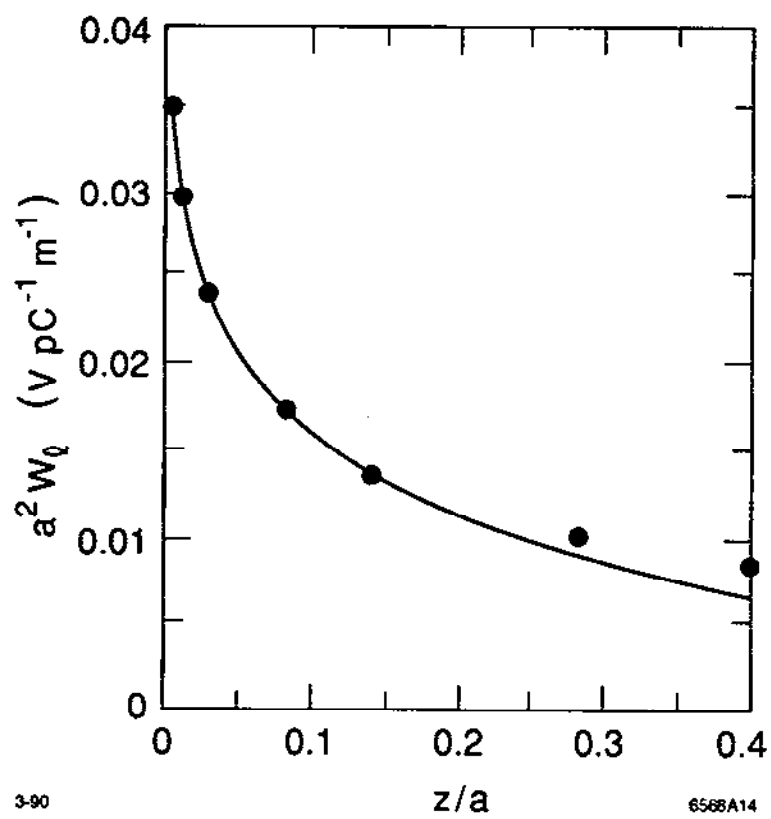


Fig. 15

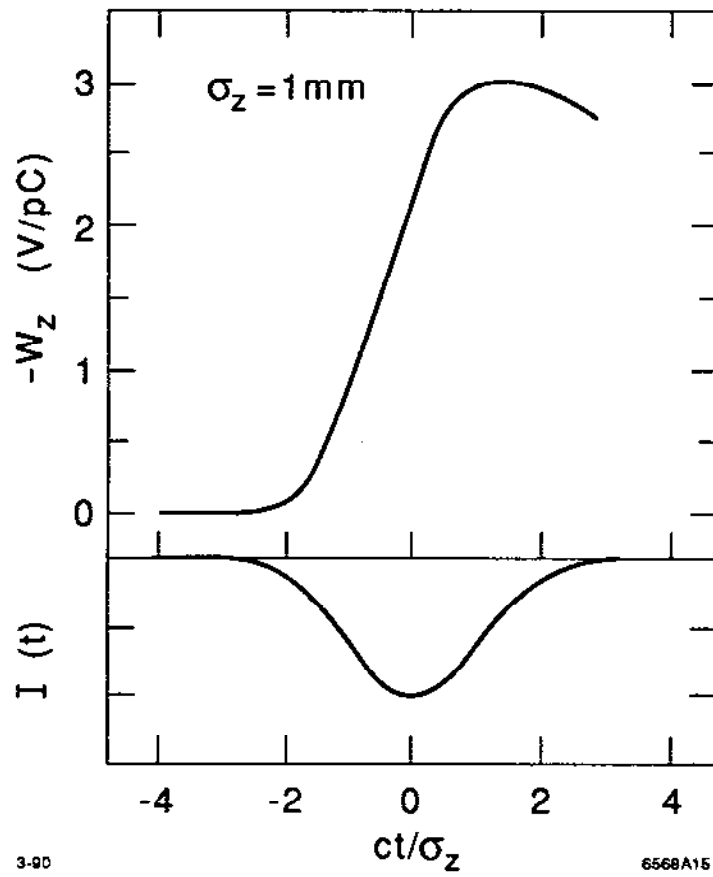
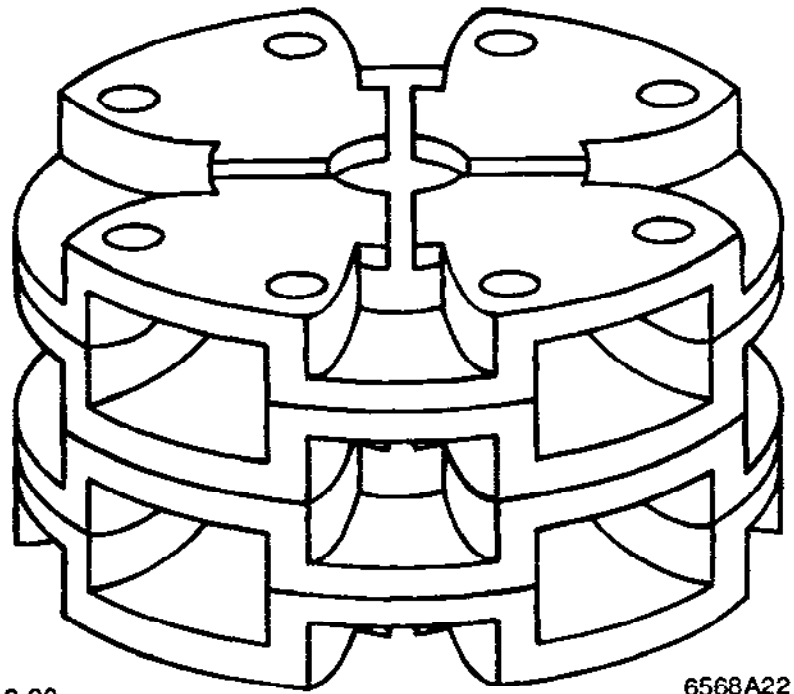


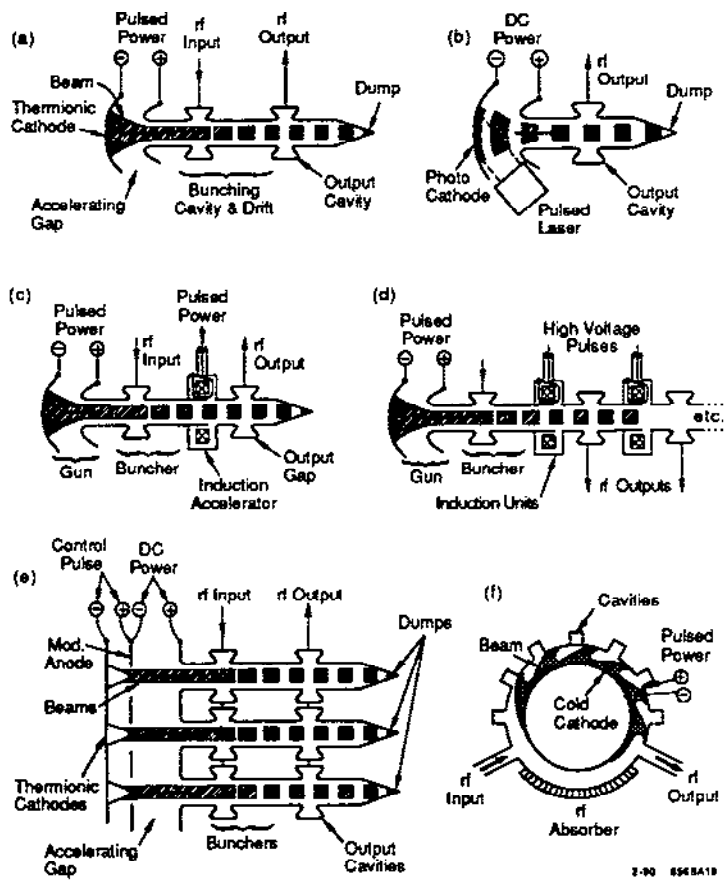
Fig. 16



3-90

6568A22

Fig. 17



2-90 8468A19

Fig. 18

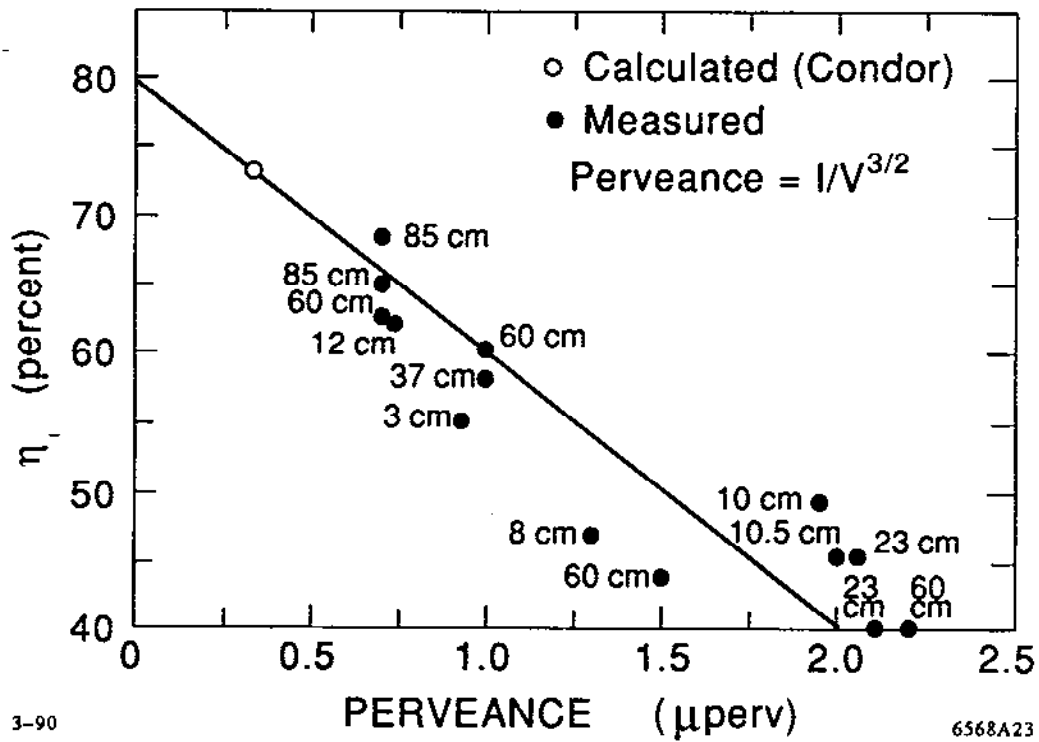
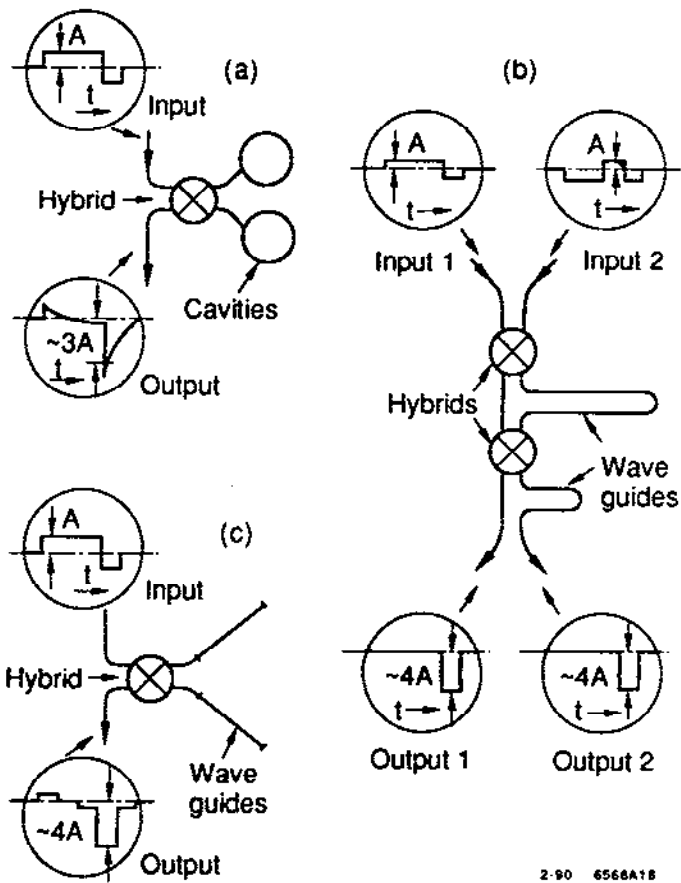
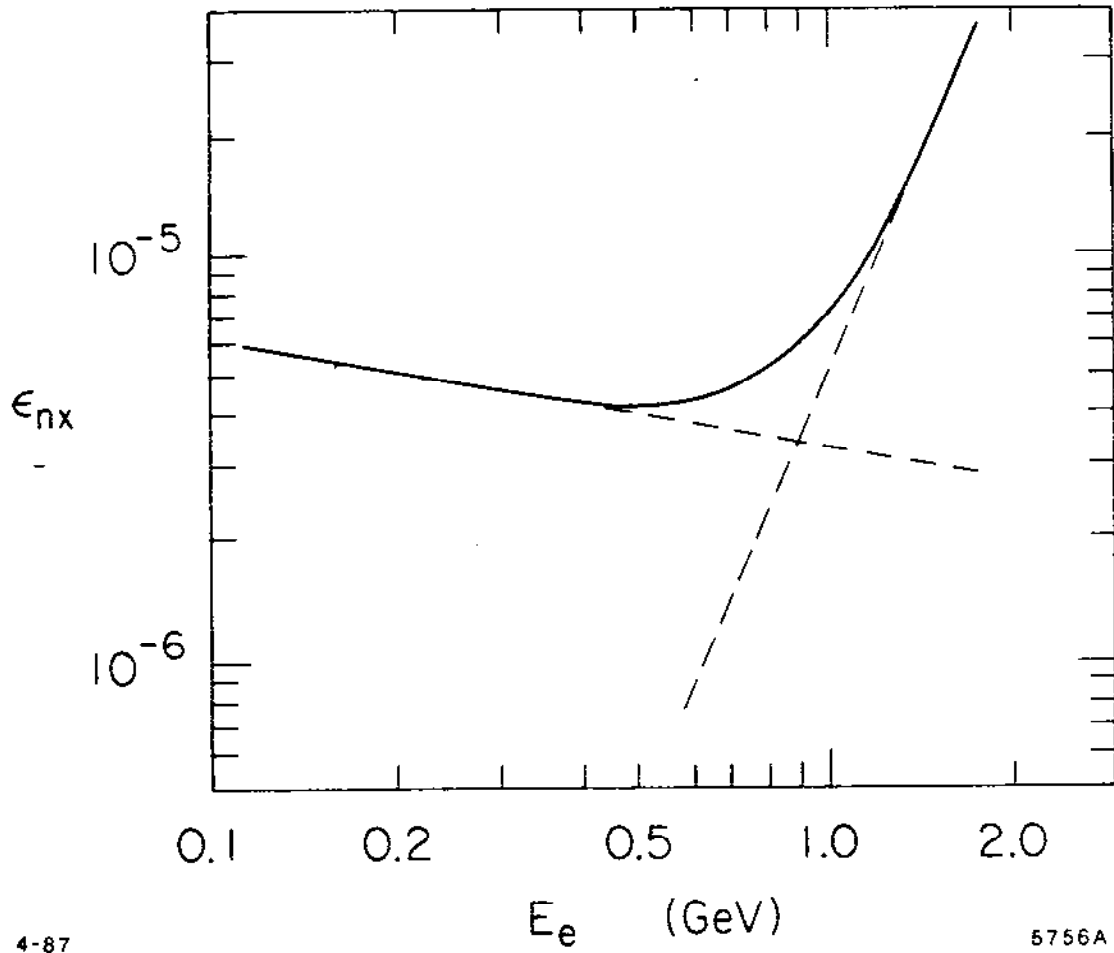


Fig. 19



2-90 6566A18

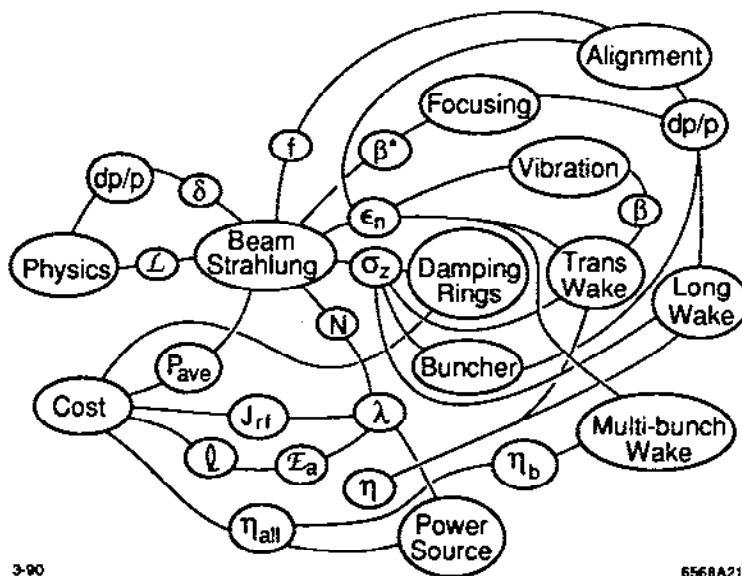
Fig. 20



4-87

5756A1

Fig 21



3-90

6568A21

Fig 22

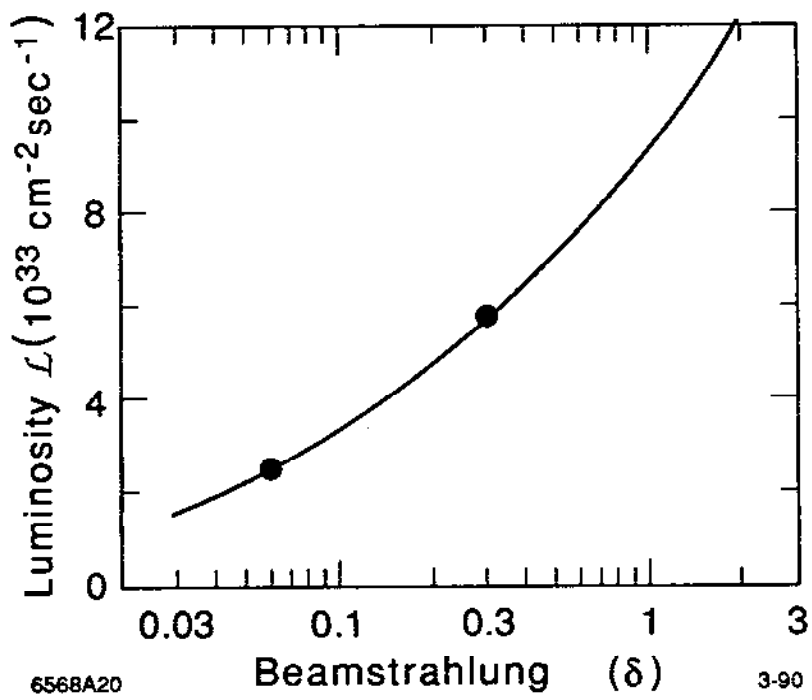


Fig. 23